

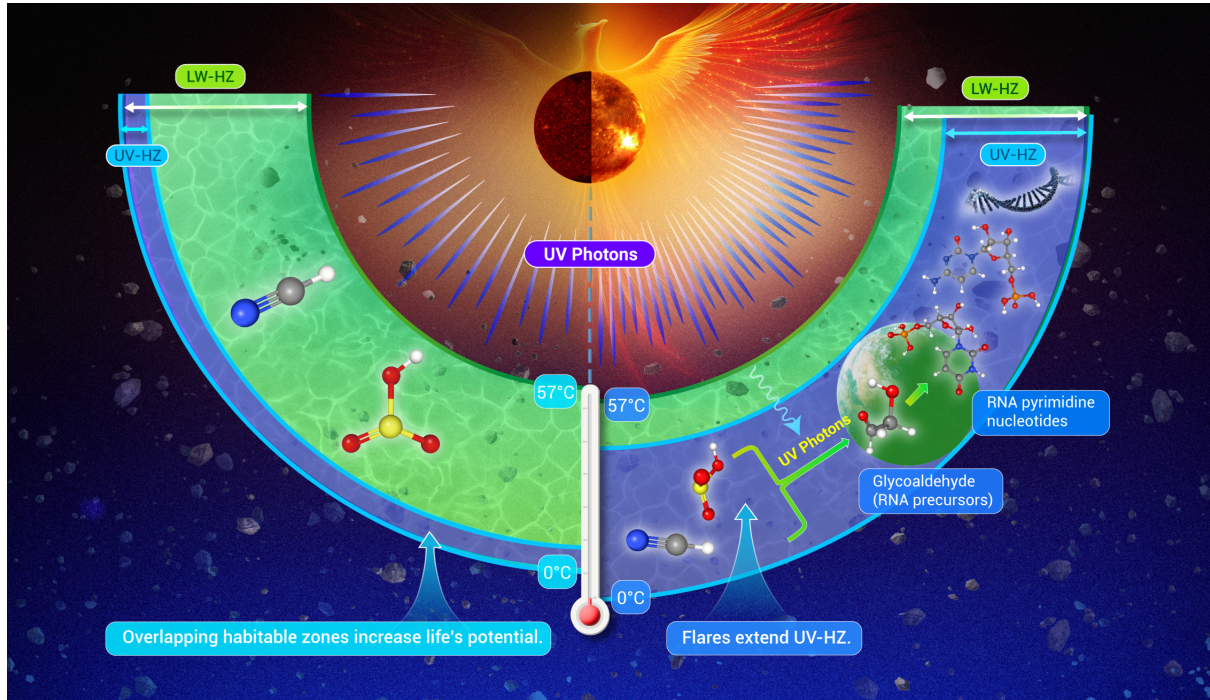
Flare-driven habitability: Expanding life's potential around low-mass stars

Dong-Yang Gao^{1,2,6}, Hui-Gen Liu^{1,4,6,*}, Ming Yang^{3,5,6,*}, and Ji-Lin Zhou^{1,4}

⁶These authors contributed equally to this work.

*Corresponding author. Email: huigen@nju.edu.cn (H.-G.L.); myang@tongji.edu.cn (M.Y.)

GRAPHICAL ABSTRACT



PUBLIC SUMMARY

- An improved flare spectrum model evaluates the effect of stellar flares on planetary habitability.
- Photochemical reaction rates varying with temperature constrain a physical ultraviolet habitable zone (UV-HZ).
- Flares extend the HZ around low-mass stars to sustain both liquid water and prebiotic UV environments.
- One rocky planet around *Kepler* flaring stars is identified in the UV-HZ and is worth further observation.

Flare-driven habitability: Expanding life’s potential around low-mass stars

Dong-Yang Gao^{1,2,6}, Hui-Gen Liu^{1,4,6,*}, Ming Yang^{3,5,6,*}, and Ji-Lin Zhou^{1,4}

¹School of Astronomy and Space Science, Nanjing University, Nanjing, 210023, China

²Shandong Key Laboratory of Space Environment and Exploration Technology, Institute of Space Sciences, School of Space Science and Technology, Shandong University, Weihai, 264209, China

³College of Surveying and Geo-Informatics, Tongji University, Shanghai, 200092, China

⁴Key Laboratory of Modern Astronomy and Astrophysics, Ministry of Education, Nanjing, 210023, China

⁵Shanghai Key Laboratory for Planetary Mapping and Remote Sensing for Deep Space Exploration, Shanghai, 200092, China

⁶These authors contributed equally to this work

*Correspondence: huigen@nju.edu.cn (H.-G.L.); myang@tongji.edu.cn (M.Y.)

ABSTRACT

The traditional definition of the circumstellar habitable zone (HZ) focuses on liquid water, but neglects the crucial role of ultraviolet (UV) radiation in prebiotic chemistry. Low-mass stars typically emit insufficient UV radiation for photochemistry throughout the liquid water HZs during quiescent states. However, frequent flares can provide substantial UV fluxes, potentially fostering habitable conditions. We refine the concept of a UV habitable zone (UV-HZ) by incorporating a temperature-dependent model for RNA precursor synthesis. Furthermore, we explore a parameterized spectral energy distribution model and adopt an empirical flare frequency distribution for flares on different stars to quantify their UV contribution. Applying this framework to different flaring stars, we find the UV-HZ around low-mass stars can extend to inner regions, and overlap with the traditional HZ in wide ranges. Apply the analysis to 9 planets around *Kepler* flaring stars, three planets are located within both the refined UV-HZ and liquid water habitable zone (LW-HZ) without causing ozone depletion. Our findings highlight the significant role of flares in expanding the potential for life around low-mass stars, offering a revised perspective on exoplanet habitability criteria.

INTRODUCTION

Detecting habitable planets has been a primary objective of the astronomical community for decades. Recent discoveries of numerous exoplanets have revealed various planetary architectures, with a higher prevalence of terrestrial worlds over giant planets.¹ To assess the habitability of the terrestrial planets, it is essential to gain a deeper understanding of their intrinsic properties and the characteristics of their host stars.² A critical aspect of this assessment is the potential for the rocky planets to sustain liquid water on their surfaces, which defines the liquid water habitable zone (LW-HZ).³

Searching for exoplanets in the habitable zone is crucial for identifying promising targets for follow-up observations and understanding their planetary properties.^{4,5} Previous studies have defined the conservative habitable zone’s boundaries through simulations of water loss and the maximum greenhouse effect, while the optimistic habitable zone is based on empirical criteria from “Recent Venus” and “Early Mars”.^{3,6} However, these definitions primarily consider the star’s steady incident flux and overlook the ultraviolet (UV) radiation, which is particularly significant for stars with frequent high-energy flares.

Excessive UV radiation can inhibit photosynthesis and damage biological systems, while moderate UV radiation supports essential biological processes.^{7,8} According to the ‘Principle of Mediocrity’, Buccino et al.⁸ proposed that planets in the UV radiation habitable zone (UV-HZ) should receive a UV flux between half and twice that of early Archean Earth. Since pyrimidine RNA precursors are essential building blocks for life, understanding the pathway to form pyrimidines is crucial.^{9,10} This pathway

involves seven steps with similar photochemical rate constants, starting from a mixture of HCN and SO_3^{2-} or HS^- . Rimmer et al.¹⁰ estimated the amount of UV light for photochemistry by experimentally measuring the rate constants for UV-driven photochemical reactions (light chemistry, required for prebiotic synthesis) and bimolecular reactions occurring in the absence of UV light (dark chemistry). They selected the region where UV radiation ($>45 \text{ erg cm}^{-2} \text{ s}^{-1}$) can provide at least 50% yield per step, resulting in an overall yield ($>0.1\%$) sufficient to sustain stable prebiotic chemical reactions. According to the Arrhenius Equation,¹¹ chemical reaction rates are highly sensitive to temperature. Rimmer et al.¹⁰ also provide the NUV (200-280 nm) flux required for abiogenesis at different temperatures, referred to as the abiogenesis flux (f_{Abio}).

As stellar temperature (T_{eff}) decreases with decreasing stellar mass, UV radiation from low-mass stars is weaker. Thus, quiet low-mass stars may not provide sufficient UV energy for synthesizing biological mechanisms within the liquid water habitable zone.^{12,13}

Since many low-mass stars are more magnetically active, these flares, caused by magnetic reconnection on the stellar surface, release bolometric radiation¹⁴⁻¹⁶. The flares also emit enhanced UV radiation compared to their quiescent stages,¹⁷⁻¹⁹ which may support biogenetic processes.⁹ However, frequent superflares can deplete the ozone layer, allowing much more harmful UV doses to reach the planetary surface and damage proteins and lipids.^{20,21} This raises a critical question: Is the UV radiation moderate due to stellar flares, to sustain the habitable zone around low-mass stars? Understanding habitability, especially for planets around low-mass flaring stars, requires more information about the UV radiation and flare frequency of the host star.

The flare frequency distribution (FFD) is a key indicator of stellar magnetic activity and crucial for assessing planetary habitability due to flares.^{17,22} However, instrument precision and observational cadence can lead to incomplete detection of low-energy flares.^{18,23} Additionally, the lack of simultaneous multi-wavelength observations introduces significant inaccuracies in modeling flare spectral energy distributions (SEDs).^{19,24} These limitations hinder accurate FFD determination for different stars. To estimate total flare energy and obtain flare SEDs from optical light curves, both radiative-hydrodynamic simulations and empirical models are used.^{25,26}

In this study, we focus on flaring stars, which exhibit frequent flare events that boost UV and bolometric radiation on orbiting planets. We reassess the UV-HZ around these stars using an empirical and corrected cumulative FFD (CFFD) for different stellar masses and also construct an SED model for stellar flares in the NUV band. Unlike previous studies,^{13,27} we provide a more comprehensive approach by considering both the minimum requirements of UV radiation that vary with planetary surface temperatures and improving the estimation of UV-HZ boundaries based on the UV radiation required for RNA precursor synthesis. Additionally, we apply our methods to known *Kepler* planets around flaring stars to evaluate their habitability. This paper aims to identify which types of flaring stars can sustain temperate regions where liquid water and moderate UV radiation can enable the synthesis of genetic molecules or organisms.

MATERIALS AND METHODS

Flare SED model for different flaring stars

The flare spectral energy distributions (SEDs) are generated via both thermal and non-thermal mechanisms, depending on various environments, e.g., the local magnetic structure, local plasma conditions, and the rate of energy deposition.²⁸⁻³⁰ These SEDs are expected to explain the observed emissions and provide clues to physical processes in solar and stellar flares. We collect the characteristics of flare SEDs as follows:

1. Continuum radiation in the optical and NUV wavebands during flares is thought to be the response of the atmospheric heating, magnetic energy release, and electron acceleration at coronal altitudes.³¹ The hot-blackbody assumption (a thermal photospheric spectrum with $T \approx 9,000 \text{ K}$) is

able to replicate some spectral regions of flare spectra (e.g., the white-light band), while ignoring emission lines.³² The NUV continuum is significantly higher than the hot-blackbody assumption, likely caused by hydrogen recombination.¹⁹

2. Hydrogen Balmer lines are enhanced and broadened during flares, particularly in the NUV band. Below the Balmer jump wavelength (at $\sim 0.365 \mu\text{m}$), flare fluxes can increase by several times compared to predictions from hot-blackbody models. However, only a few solar flares exhibit obvious Balmer jump.³³
3. Emission lines contribution, especially in the NUV band, is non-negligible.^{24,34} Fortunately, this contribution can be included by integrating the hot-blackbody spectrum with an appropriate pseudo-continuum temperature.¹⁹

Several flare SED models based on the 9,000 K hot-blackbody spectrum, combined with the FUV and NUV emission lines taken by Hubble Space Telescope (HST), better match actual observations than the hot blackbody model (e.g., the MUSCLES model²⁶). Based on the research of TESS white light flares for M dwarfs, and combined with the GALEX UV photometric data, Jackman et al.¹⁹ extrapolated stellar FFD at the UV-band to test different flare SED models. They found that the GALEX NUV (0.177-0.283 μm) energies on M0-M2 stars predicted by the 9,000 K hot-blackbody model are underestimated by up to a factor of 2.3 ± 0.6 . More accurate SED of flares requires multiple waveband observations for each event, including low-energy flares.^{35,36}

To improve the flare SED model on various star types, we employed a power-law continuum superimposed with a hot-blackbody spectrum from 0.100 to 0.365 μm in the UV band and a hot-blackbody model in the white-light band, considering the Balmer jump. Our flare SED model is described by Equation (1),

$$F_{\lambda}(T_{\text{flare}}) = \begin{cases} F_{\lambda, \text{HBB}}(T_{\text{flare}}), & \text{for } \lambda > 0.365 \mu\text{m}, \\ F_{\lambda, \text{HBB}}(T_{\text{flare}}) + F_{0.365 \mu\text{m}, \text{HBB}}(T_{\text{flare}}) \times f_b \times \left(\frac{\lambda}{0.365 \mu\text{m}} \right)^{\gamma}, & \text{for } 0.1 \mu\text{m} \leq \lambda \leq 0.365 \mu\text{m}, \end{cases} \quad (1)$$

where $F_{\lambda, \text{HBB}}(T_{\text{flare}}) = B_{\lambda}(T_{\text{flare}}) + S_{\lambda}$, i.e. the combination of the hot-blackbody spectrum $B_{\lambda}(T_{\text{flare}})$, and the stellar spectra at quiet state S_{λ} . T_{flare} is the temperature of the stellar flare active region. The factor f_b is the enhancement ratio at 0.365 μm , and γ is the power-law index related to the wavelength dependency.

We set T_{flare} to 9,000 K, leaving two parameters for the flare SED model: the enhancement of the continuum at wavelengths shorter than the Balmer jump (f_b), and the power-law index (γ) describing the UV continuum trend. This model corrects the underestimation of UV radiation using the 9,000 K hot-blackbody assumption.^{19,24}

Stellar and solar flares are manifestations of magnetic activity and share a similar physical process.³⁷ However, on stars of different masses, with varying convective layer thicknesses, flares exhibit distinct characteristics.^{31,38} We fitted f_b and γ with observations and spectrum model of M and G stellar flares, and use linear interpolation to model the SED for different types of stars (see Table S1 in the Supplemental Information).

Figure 1 shows several flare SED models. Previous observations^{19,33} indicate that for M stars, f_b is higher than for solar flares, while γ is lower. This suggests that UV-optical radiation contrast during flares is more pronounced on M stars compared to G and K stars. In our model, as T_{eff} ranges from 3,400 K to 6,000 K, $f_b(T_{\text{eff}})$ varies from 1.013 to 0.011, and $\gamma(T_{\text{eff}})$ from -0.500 to 1.032 (see Figure S1 in Supplemental Information). Note that this work investigates changes in the habitable zone considering flares for specific spectral types. Therefore, f_b and γ represent the typical or average flare SED for a stellar type, not an individual star. The energy range for detected solar and stellar flares spans from 10^{28} to 10^{38} erg.^{17,23,39,40} Details on our flare SED model validation and the increase in stellar luminosity

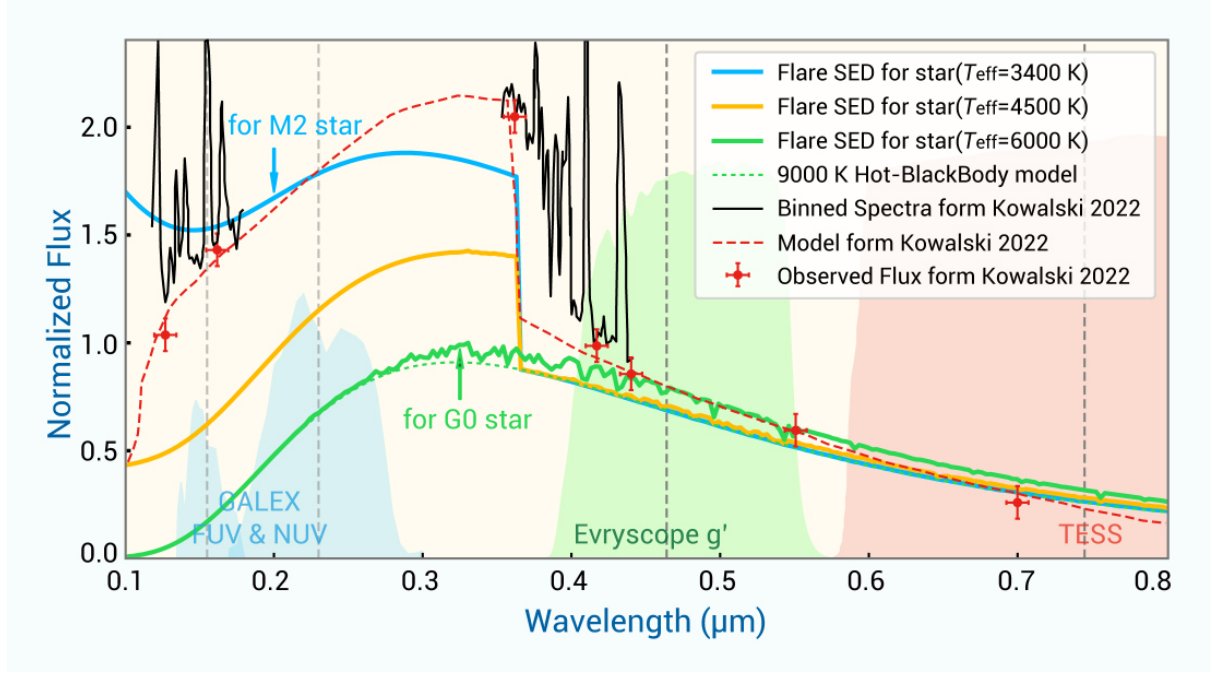


Figure 1. Flare SEDs on different spectral types. The blue, orange, and green solid lines represent flare SED models for stars with different effective temperatures of 3,400 K, 4,500 K, and 6,000 K, respectively. Two arrows highlight the flare SEDs for M2 ($T_{\text{eff}} = 3,400$ K) and G0 ($T_{\text{eff}} = 6,000$ K) type stars, respectively. For stars with $T_{\text{eff}} < 6,000$ K, flares can enhance the NUV band compared to the $T_{\text{flare}} = 9,000$ K hot-blackbody model (the green dotted line). The black solid line represents the “great flare” spectra of AD Leo, with points with error bars marking its wavelength-binned observed continuum fluxes from Kowalski.²⁵ The brown dashed line is the best fit using a two-component radiative-hydrodynamic model from the same study. Colored backgrounds show the relative band-passes of different filters, with gray vertical dashed lines marking the mean wavelengths for GALEX FUV band ($0.155 \mu\text{m}$), GALEX NUV band ($0.230 \mu\text{m}$), Evryscope g' band ($0.464 \mu\text{m}$), and TESS band ($0.745 \mu\text{m}$).

due to flares are in Section “Average luminosity of flaring stars” in the Supplemental Information. The averaged stellar NUV radiation is a necessary condition for the accumulation of photochemical reaction products, which are essential for forming the macromolecular prebiotic inventory (see “Habitable zones around different flaring stars” subsection for details).

Calculation of Habitable Zone around Flaring Stars

Liquid Water Habitable Zone

For quiet stars, the LW-HZ boundaries are determined using the methods of Kopparapu et al.^{3,6} The inner boundary corresponds to “recent Venus” at 57 °C,⁴¹ and the outer boundary to “early Mars” at 0 °C. For flaring stars, stellar flares increase the flux reaching the planet. Although magnetic active regions are randomly distributed across the stellar surface, only flares directed towards the planet affect its habitability. We calculated the increase in stellar luminosity caused by flares, as detailed in the Supplemental Information. Considering existing flare spectra and the SEDs for M to G stars, the integrated wavelength range is set from 0.1 to 3.0 μm .

By adjusting the LW-HZ boundaries for quiet stars considering the increased stellar bolometric luminosity, we determined the LW-HZ boundaries for flaring stars. This adjustment is uniformly applied to both the inner and outer limits,

$$d_{\text{flare, LW}} = d_{\text{quiet, LW}} \times \left(1 + \frac{L_{\text{flare}}}{L_*}\right)^{0.5}, \quad (2)$$

where $d_{\text{flare, LW}}$ is the distance from the host star to the boundary of LW-HZ when considering stellar flares, and $d_{\text{quiet, LW}}$ is the distance from the host star to the boundary of LW-HZ without considering stellar flares. L_{flare} is the time-averaged bolometric luminosity of the star with stellar flares (as explained with Equation S6 in the Supplemental Information), and L_* is the bolometric luminosity in the quiescent state.

Ultraviolet Radiation Habitable Zone

The Ultraviolet Radiation Habitable Zone (UV-HZ) mainly focuses on biological processes. On the Archean Earth about 3.8 billion years ago, NUV radiation provided essential energy sources for synthesizing biochemical compounds. Previous studies defined the UV-HZ considering the UV flux required for abiogenesis only at 0 °C. However, according to the Arrhenius Equation^{10,11}, chemical reaction rates are highly sensitive to temperature. On planets like Earth, with an average temperature of 15 °C, reaction rates significantly increase. Consequently, more UV radiation is needed to sustain RNA synthesis.

To obtain the average NUV flux required for abiogenesis (f_{Abio}), we fitted the relationship between f_{Abio} and the planet surface temperature (T_{surf}) using the Arrhenius Equation, according to Figure 3A in Rimmer et al.¹⁰ Similarly, we chose the 50% curve from the figure to ensure sufficient flux for robust prebiotic chemistry. The fitting results are as follows:

$$f_{\text{Abio}} = f_0 \times e^{(T_{\text{surf}} - 273 \text{ K})/10 \text{ K}} \text{ photons cm}^{-2} \text{ s}^{-1}, \quad (3)$$

where $f_0 = 4.08 \times 10^{12}$.

The surface equilibrium temperature T_{surf} is proportional to $d^{-0.5}$, if we ignore the atmospheric greenhouse effect of a planet. However, when considering the planet’s atmosphere, the temperature decrease with distance is less significant. To model the correlation between T_{surf} and d , we adopted an exponential function:

$$T_{\text{surf}} = T_0 \left(\frac{d}{1 \text{ AU}}\right)^\chi. \quad (4)$$

To determine T_0 and χ in Equation (4), we use the inner and outer boundaries of the LW-HZ defined by Kopparapu et al.^{3,6} The inner boundary is set at the Moist Greenhouse limit, where the surface

temperature is set as 330 K,⁴¹ while the outer boundary is at the freezing point of water ($T_{\text{surf}} = 273$ K). By comparing these boundary temperatures (i.e. T_{surf}) with their respective distances (i.e. d), we can derive the value of χ using Equation (4) for different stars. In the case of a solar-type star, $T_0 = 310.12$ K and $\chi = -0.22$. Consequently, by substituting Equation (4) into (3), and adopting the first order approximation, we have $f_{\text{Abio}} \propto d^{-7}$ within the LW-HZ. Figure 2 shows the f_{Abio} and modeled surface temperatures at different locations for typical M, K, and G stars.

To obtain the quiescent NUV flux of different stars, stellar photospheric models (e.g., PHOENIX^{42,43}) are usually adopted, which only include stellar photospheric radiation. However, radiation contributions from the chromosphere and transition region cannot be neglected. Especially for cooler stars (K to M stars), the photospheric flux between 200 and 280 nm is relatively weak in comparison to chromospheric emission.⁴⁴ To account for contributions from other mechanisms, we corrected the NUV flux obtained from the PHOENIX model by dividing by different factors. These factors are the fraction of modeled radiation to observed radiation in the GALEX NUV band (0.177-0.283 μm). We calculated the median factors for different stars according to the statistic sample in Wang et al.⁴⁵ (see Figure S3). After correction, the total NUV radiation of different stars in the quiescent stage can be obtained, including contributions from the photosphere, chromosphere, transition region, and corona.

To estimate the contribution of NUV due to stellar flares, we adopted the flare SED model and the empirical CFFD based on a sample of young stars ranging from G to M types¹⁸. We calculated the total energy of flaring stars over a long-term period and added the time-averaged increase in NUV flux to the quiescent stellar flux (see “[Enhancement of stellar luminosity caused by flares](#)” in Supplemental Information). Note the NUV enhancement due to stellar flares is time-dependent. The typical timescale of flare events is several hours. According to previous studies, the reaction timescales of certain prebiotic precursor molecule, like 2-aminooxazole, range from minutes to hours.⁴³ However, for planetary atmosphere or surface, the subsequent chemistry of the products is often coupled with the global dynamics of materials, which typically operate on timescales much longer than flare durations. For instance, the global impact of stellar flares on the atmospheric ozone column depth can last for months to years, according to Segura et al.⁴⁶ Thus, adopting the time-averaged increase due to stellar flares can represent the secular and global influence on photochemistry.

After obtaining the averaged NUV flux of flaring stars, we used the lower limit of f_{Abio} to estimate the UV-HZ boundary. By comparing the average stellar insolation and f_{Abio} (see Equation 3) above the planet’s atmosphere at different distances and surface temperatures, we determined the inner boundary of UV-HZ with and without flares (see Figure S7 in Supplemental Information). As the distance from the star decreases, the abiogenesis flux rapidly increases ($f_{\text{Abio}} \propto d^{-7}$ for solar-type stars), while stellar radiation increases more gradually ($\propto d^{-2}$). Therefore, there is a physical inner boundary of UV-HZ to guarantee the minimum requirements of f_{Abio} . Beyond the inner boundary, stellar radiation consistently meets the abiogenesis flux required for life (see Figure 2, Figure S6 and S7 in Supplemental Information). Considering the need for liquid water to support life, the outer boundary of UV-HZ is therefore set to align with the outer boundary of LW-HZ.

The limits of CFFD for ozone depletion

Since the inner boundary of UV-HZ is defined by the lower limit of UV flux, there should also be an upper limit of the UV flux, as excessive UV radiation can dissociate prebiotic molecules. According to Abrevaya et al.,⁴³ even if the received UVC (200-280 nm) flux is ~ 15 times higher than the current Earth’s flux outside the atmosphere (i.e. 92 W m^{-2}), a small fraction ($\sim 10^{-4} - 10^{-5}$) of microorganisms can still survive. However, this UVC flux refers to radiation outside the atmosphere. Since atmospheric components, such as ozone, have varying abilities to shield UV radiation, the surface UV flux should be lower than the estimated flux outside the atmosphere. Furthermore, UV-photounstable molecules can extend their lifetimes through a self-shielding mechanism (e.g., 2-aminooxazole) or the presence of other UV-absorbing molecules (e.g., purine ribonucleosides).⁴⁷ Additionally, turbid water containing UV-absorbing species (e.g., $\text{Fe}(\text{CN})_6^{4-}$) can strongly shield UV radiation.⁴⁸ Thus, some molecules dissolved

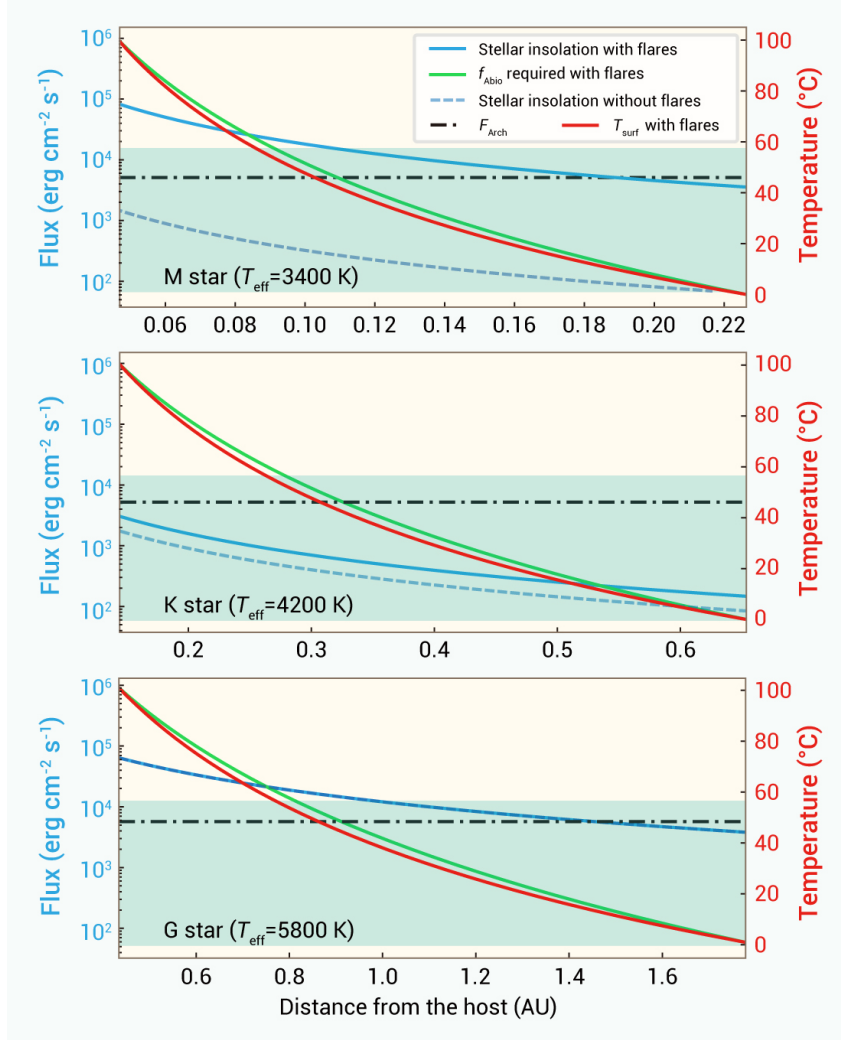


Figure 2. The required NUV flux for prebiotic chemistry in LW-HZ around typical **M**, **K**, and **G** stars. The green solid line represents the f_{Abio} requirements at different locations, while the blue solid and dashed lines represent the stellar NUV insolation with and without flares, respectively. The inner boundary of the UV-HZ is the intersection of the green and blue solid lines. The NUV flux of Archean Earth (F_{Arch}) is also shown using a dot-dashed line. The red line shows the variation of modeled surface temperature (T_{surf}) on the planet, and the green background marks the region with temperatures between 0°C (273 K) and 57°C (330 K).

or accumulated in water may be preserved. We therefore did not really use the upper limit on UV flux via prebiotic chemistry.

However, for mature planetary systems, such as terrestrial planets around *Kepler* flaring stars, ozone in Earth-like atmospheres becomes crucial for shielding UV radiation and protecting potential life. Thus, we constrained the CFFD of superflares based on previous studies to avoid significant ozone depletion. Frequent superflares can severely deplete the ozone layer via energetic particles and UV radiation. An Earth-like ozone layer around M dwarf stars like GJ1243 would be greatly depleted by flares of 10^{34} erg at a frequency of 0.4 day^{-1} .^{17,21} Therefore, we scaled an upper limit on CFFD to account for ozone depletion. I.e., if the CFFD of a given flaring star exceeds $10^{34} \times (\frac{d}{0.16 \text{ AU}})^2$ erg flares, the planet is considered inhabitable. d represents the distance between the planet and host stars. Fortunately, all the empirical CFFDs adopted for different stars are below these upper limits, even when considering the uncertainties in the fitted correlations.

RESULTS

Habitable zones around different flaring stars

Life on Earth originated 3.8 Gyr ago,⁴⁹ when the Sun was approximately 0.8 Gyr old. Therefore, a timescale of ~ 1.0 Gyr is required for life to originate.^{50,51} Chromospheric activity and coronal emission of G, K, and M stars gradually keep a high level before 1 Gyr and decrease due to the reduced dynamo production of magnetic fields as the star spins down.⁵² It's hard to know when the prebiotic molecules can be produced for Archean Earth, but the M stars with longer lifetime in the main-sequence stage can have adequate time to accumulate the prebiotic molecules when the UV radiation becomes moderate. To estimate the NUV radiation of young stars during life origination, we selected 1.0 Gyr as the typical age for calculating stellar insolation.

For the general case, we consider flaring stars ranging from 0.3 to 1.1 solar masses (M_{\odot}), spanning spectral types M2 to G0. We employed the stellar evolution model at 1.0 Gyr age from Baraffe et al.⁵³ to calculate the effective temperature (T_{eff}) and radius (R_{*}) of these stars. Using flaring samples from Gao et al.,¹⁸ we established an empirical relationship between the CFFD and T_{eff} , and calculated the HZ boundaries considering the averaged luminosity of flaring stars. More calculation details can be found in “[MATERIALS AND METHODS](#)” Section.

As shown in Figure 3, the UV-HZ always exists around early K and G-type stars ($M_{*} = 0.76\text{--}1.10 M_{\odot}$, $T_{\text{eff}} = 4,700\text{--}6,000 \text{ K}$), regardless of flares. Considering the quiescent stellar NUV radiation, including contributions from the photosphere, chromosphere, transition region, and corona, the UV-HZ is narrow (e.g., less than 0.007 AU for a quiet star below $\sim 0.36 M_{\odot}$), and the planet can hardly be located inside. If only considering the NUV flux contributed by the photosphere, the UV-HZ disappears for quiet stars below $\sim 0.76 M_{\odot}$. However, if the star has flares, the increased UV flux can extend the UV-HZ. For G-type flaring stars, the UV-HZ extends slightly because the enhancement of UV flux due to flares is only a small fraction of quiescent radiation. Due to a higher flare frequency, the UV-HZ extends more noticeably for lower-mass stars. Additionally, K-type stars around $0.68 M_{\odot}$ exhibit a narrow UV-HZ. Notably, the flare SED significantly enhances NUV luminosity rather than the total luminosity; thus, the LW-HZ experiences negligible change ($< 0.006 \text{ AU}$) across all stellar types.

To assess the impact of flare SED models on UV-HZ changes, we examined two specific flare SEDs: the G0-type flare SED, which includes only the traditional 9,000 K hot-blackbody assumption, and the M2-type flare SED, which accounts for the Balmer jump of flares on M-type stars and is thus more accurate. As shown in Figure S9, although the UV-HZ range using the M2-type flare SED is significantly larger, both SEDs can extend the UV-HZ obviously, and lead to a wide overlapping range with LW-HZ.

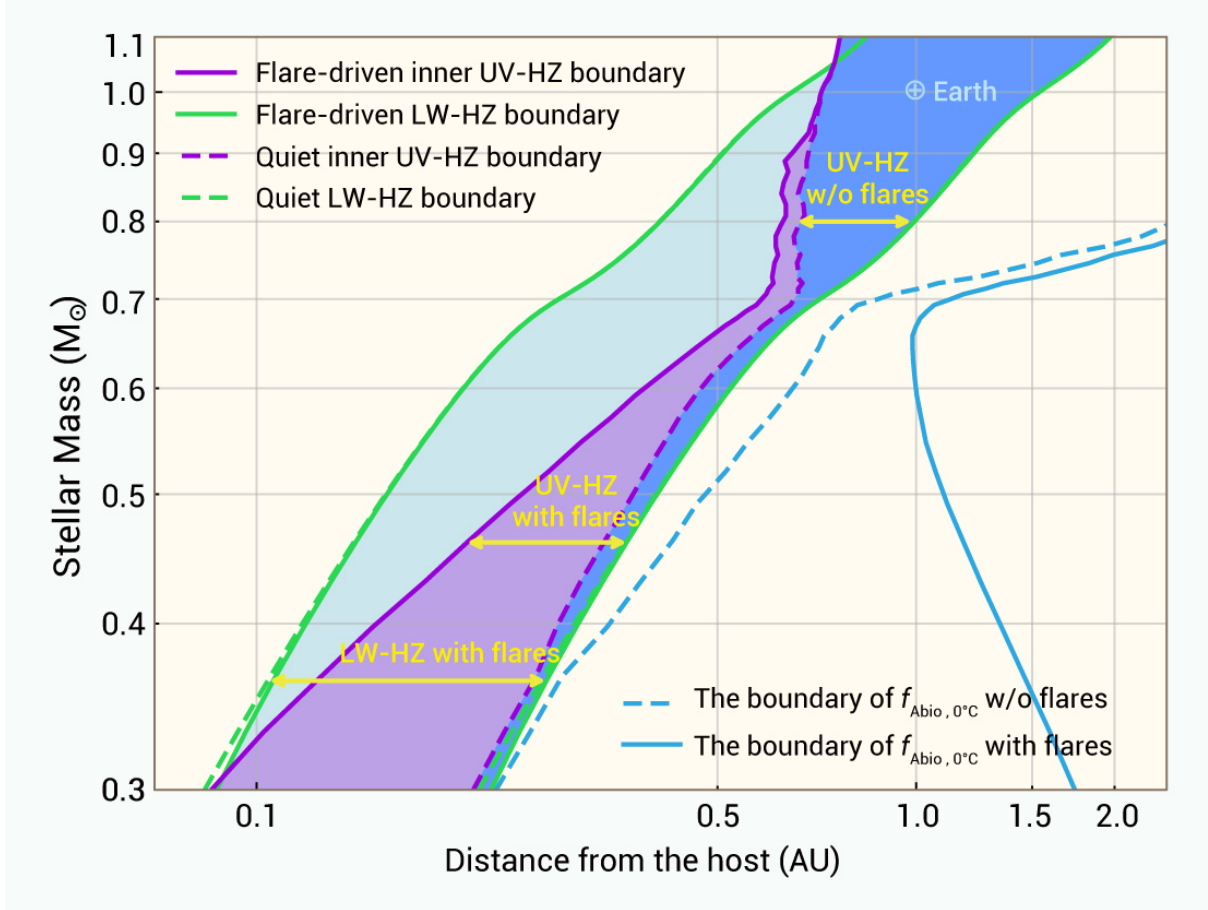


Figure 3. The habitable zones (HZs) around flaring stars at the age of 1.0 Gyr. The magenta solid line indicates the flare-driven inner UV-HZ boundary, while the magenta dashed line shows the quiet inner UV-HZ boundary. The lime solid line indicates the flare-driven LW-HZ boundary, while the lime dashed line shows the quiet LW-HZ boundary. The boundary of the flux required for abiogenesis at 0°C without (w/o) and with flares is plotted as blue dashed and solid lines, respectively. Considering that prebiotic chemistry also requires a liquid water environment, we adopt UV-HZ with the same outer boundary as LW-HZ. The position of Earth is also marked with a circled cross in the figure.

Habitable zones around *Kepler* flaring hosts

Yang and Liu²³ presented a catalog of *Kepler* flaring stars, including five with planetary candidates and four with confirmed exoplanets listed as habitable planetary hosts in the NASA Exoplanet Archive [<https://exoplanetarchive.ipac.caltech.edu/>]. Their habitability is defined by an equilibrium temperature of 180 K to 310 K or received insolation between 0.25 and 2.2 times that of Earth.

Using the stellar and planetary parameters (see Table S4 in Supplemental Information), we calculated the LW-HZ boundaries based on Equation 3 from Kopparapu et al.³ We performed flare detection on the *Kepler* lightcurves of these hosts, and fitted the CFFD parameters for each star (see Table S3 in the Supplemental Information). We measured the NUV radiation flux of five hosts using GALEX NUV data (see Table S4). For four hosts without GALEX NUV or Swift UVOT observations, we adopted their NUV radiation flux as the statistical median values from Wang et al.⁴⁵ (see Figure S3). For the Sun, we adopted 1.4 times the modern solar spectrum from Willmer⁵⁴ to account for the NUV radiation evolution of G-type stars with an age of 1.0 Gyr.⁵⁵ We then derived the LW-HZ and UV-HZ boundaries, considering both the presence and absence of stellar flares. Figure 4 shows the changes in stellar insolation and the changes in the habitable zone boundary before and after considering flares around Kepler-438. During the quiescent stage, the UV-HZ is as narrow as 0.04 AU. After accounting for the enhancement of flares, the width of the UV-HZ increases to 0.16 AU, resulting in a fourfold increase in the likelihood of accommodating an additional terrestrial planet in the HZ.

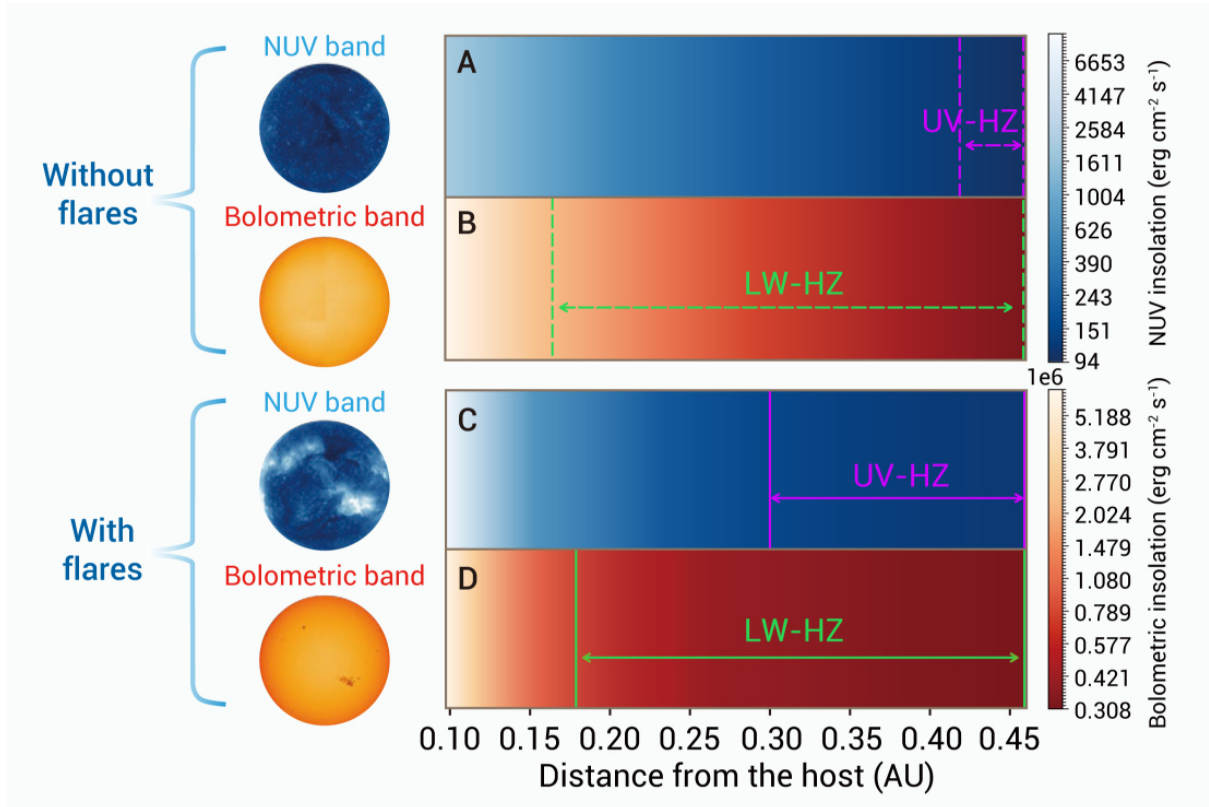


Figure 4. Stellar insolation around Kepler-438 without and with flares. Panel A shows the NUV band insolation (200–280 nm) without flares, while Panel B presents the bolometric insolation under the same quiet conditions. Panels C and D show these insolation types with flares. Lime and magenta vertical lines mark the LW-HZ and UV-HZ boundaries without/with flares, respectively.

Figure 5 illustrates the HZ boundaries of the planet hosts. KOI-7706.01 and Kepler-1512 b are no longer in the LW-HZ with updated stellar parameters (see Table S4). Although Kepler-1540 b, Kepler-438 b, and Kepler-155 c are in the LW-HZ, they are not in the UV-HZ. The three planets, i.e.,

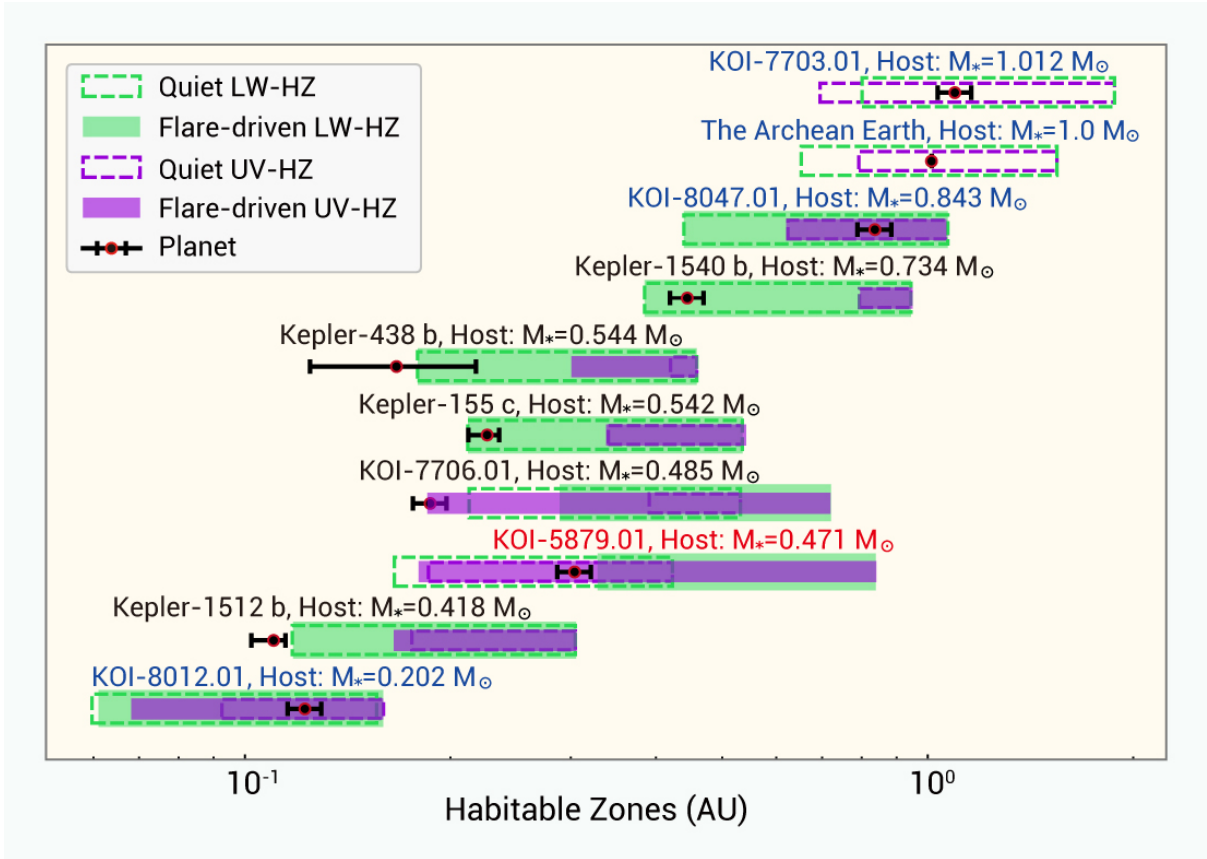


Figure 5. LW-HZs and UV-HZs sorted by stellar mass. Lime dashed boxes represent Quiet LW-HZs. Lime backgrounds represent Flare-driven LW-HZs. Magenta dashed boxes represent Quiet UV-HZs. Magenta backgrounds represent Flare-driven UV-HZs. Black dots represent planets or candidates located at their semi-major axes with errors (see Table 1). Due to unavailable CFFD power-law indices for KOI-7703 and the Archean Sun, their flare-driven HZs are not considered.

Table 1. Boundaries of the habitability zones for candidate and confirmed exoplanets orbiting *Kepler* flaring stars.

The planet	a^a (AU)	$d_{\text{in, FLW}}$ (AU)	$d_{\text{out, FLW}}$ (AU)	$d_{\text{in, FUV}}$ (AU)	located in ^b	TSM ^c
Kepler-1540 b	0.4426±0.0251	0.383	0.941	0.788	LW-HZ	2.271
KOI-7703.01 ^d	1.0911±0.0618	0.798	1.869	0.693	LW-HZ, UV-HZ	0.956
KOI-8047.01	0.8332±0.0472	0.438	1.065	0.621	LW-HZ, UV-HZ	0.576
Kepler-155 c	0.2254 ^{+0.0092} _{-0.0139}	0.211	0.533	0.333	LW-HZ	0.553
KOI-5879.01 ^e	0.3027±0.0172	0.327	0.835	0.179	-	0.332
Kepler-1512 b	0.1097 ^{+0.0045} _{-0.0079}	0.117	0.304	0.164	-	0.059
Kepler-438 b	0.1660 ^{+0.0510} _{-0.0420}	0.179	0.459	0.300	LW-HZ? ^f	0.059
KOI-7706.01 ^g	0.1860±0.011	0.288	0.719	0.185	-	0.028
KOI-8012.01	0.1219±0.0069	0.062	0.162	0.069	UV-HZ, LW-HZ	0.006
The Archean Earth ^d	1.0	0.650	1.539	0.790	UV-HZ, LW-HZ	-

Note: $d_{\text{in, FLW}}$ and $d_{\text{out, FLW}}$ denote the inner and outer boundaries of the flare-driven LW-HZ, respectively; $d_{\text{in, FUV}}$ represents the inner boundaries of the flare-driven UV-HZ. Note the outer boundaries of the flare-driven UV-HZ are set the same with $d_{\text{out, FLW}}$.

^a For KOI-8012.01 and KOI-7706.01, which lack semi-major axis uncertainty in the source reference, we applied a typical 17% uncertainty for stellar mass from Thompson et al.⁵⁶ to estimate the uncertainty via error propagation.

^b “UV-HZ” and “LW-HZ” represent the ultraviolet habitable zone and the liquid water habitable zone driven by flares, respectively.

^c The Transmission Spectroscopy Metric (TSM) is calculated following Kempton et al.⁵⁷ to assess the viability of follow-up exo-atmospheric observations.

^d KOI-7703 and the Archean Sun lack sufficient flare events to fit the CFFD. Therefore, the boundaries for scenarios without stellar flares are presented.

^e For KOI-5879, a more appropriate integration range for flare energies was chosen from 10^{30} to 10^{38} erg (see the Notice b of Table S3 for details).

^f Measurement uncertainties in the semi-major axis prevent a clear conclusion of whether this planet resides within the LW-HZ (see Figure 5).

^g Flares on KOI-7706 may potentially deplete ozone layers of KOI-7706.01 (see Figure S8). (This table is available in its entirety in machine-readable form.)

KOI-7703.01, KOI-8047.01, and KOI-8012.01, are all located in the overlapping region of the two HZs (regardless of whether flaring is considered or not). Coincidentally, these three stars are G, K, and M stars, respectively. Note that KOI-5879.01 was originally in the LW-HZ. After considering the flares, the NUV radiation can satisfy the abiogenesis flux, but it is no longer in the LW-HZ.

As described in Subsection “The limits of CFFD for ozone depletion”, we also examined the limits of CFFD for ozone depletion, based on the fitted CFFD of these 9 planet hosts via their *Kepler* light curves. The frequency of superflares with certain energy must not exceed 0.4 day^{-1} . Otherwise, such superflares would lead to ozone depletion on their planets.²¹ Figure 6 shows an example of the observed and fitted CFFD of KOI-8012, considering the constraints from the ozone depletion. For KOI-7706, its flare frequency could potentially cause ozone depletion on its planet, because the CFFD with energy of $1.35 \times 10^{34} \text{ erg}$ is very close to the limit of 0.4 day^{-1} (see the details in Figure S8).

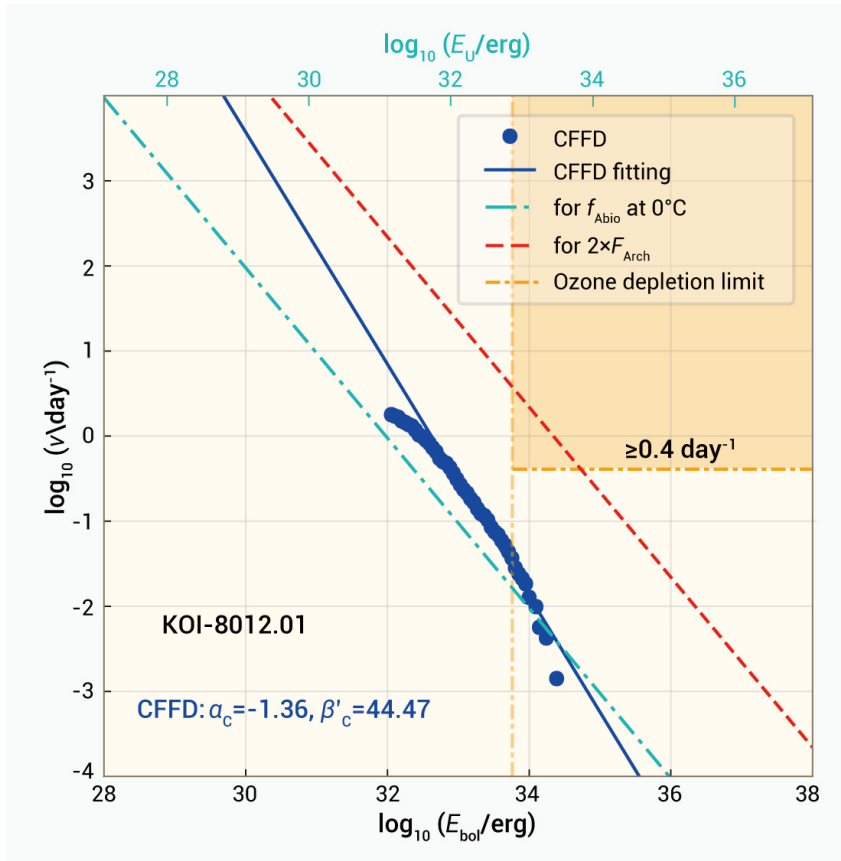


Figure 6. The Cumulative FFD (CFFD) of KOI-8012. The blue dot represents the CFFD directly from observations. The blue line illustrates the fitted CFFD, with two parameters (α_C and β'_C , in blue text) marked in the lower left corner. The orange area denotes the ozone depletion forbidden region, where flare rates are $\geq 0.4 \text{ day}^{-1}$ with flare bolometric energy larger than $0.58 \times 10^{34} \text{ erg}$. The cyan dot-dashed line represents the lower limit of flaring required by the abiogenesis flux at 0°C . The red dashed line represents the frequency for twice the NUV flux received by the Archean Earth.⁸ Note that the cyan dot-dashed and red dashed lines are only drawn in this figure for comparison with previous studies, and are not used in the definition of the UV-HZ.

In summary, the habitability of the nine planets around *Kepler* flaring hosts is as follows:

- One rocky planet (KOI-8012.01) and two super-earths (KOI-8047.01 and KOI-7703.01) are in both the UV-HZ and the LW-HZ. The CFFDs of their host stars do not exceed the limit of ozone depletion. Thus, they provide radiation environments more suitable for abiogenesis.

- Three planets (Kepler-1540 b, Kepler-438 b, and Kepler-155 c) are located in the LW-HZ. However, they are not within the UV-HZ defined by abiogenesis requirements under modeled surface temperatures. For Kepler-438 b and Kepler-155 c, if the temperature in some regions of their surface can be maintained at 0°C, the received UV radiation can satisfy the requirements for abiogenesis (see Figure S8 for more explanation).
- KOI-7706.01 and Kepler-1512 b are not located in the LW-HZ or the UV-HZ. Moreover, the CFFD of KOI-7706 nearly reaches the threshold for ozone depletion, making these two planets less likely to support prebiotic chemistry.
- KOI-5879.01 was originally within the LW-HZ and the UV-HZ if its host star were quiescent. However, flares from the host star cause an outward expansion of the LW-HZ, and it is therefore no longer within the HZ.

DISCUSSION

Although many exoplanets have been studied statistically, assessing the habitability of individual planets in the habitable zone is still challenging from both astrobiological and observational perspectives. Evaluating habitable zones around stars in various aspects helps us better understand exoplanet habitability.^{5,58} By re-evaluating the habitable zones and creating a comprehensive catalog of planets within them, we can infer that terrestrial planets in both liquid water and UV radiation habitable zones are more likely to support life.

In this paper, we highlight that the requirements of UV radiation for abiogenesis vary rapidly with temperature. According to the analysis of planets around flaring stars, we use a modeled temperature to estimate the inner boundary for UV-HZ. Since the surface temperature is correlated with different aspects, e.g., atmosphere effect, surface albedo, and thermal redistribution on day and night side.⁵⁹ Thus, Kepler-1540 b, Kepler-438 b, and Kepler-155 c deserve further investigation by large telescopes to better constrain their temperatures. Even KOI-7703.01, KOI-8047.01, and KOI-8012.01, which are among the most promising targets, need to be characterized in terms of their atmospheric properties. We also calculate the TSM of these planets, as shown in Table 1.

An averaged UV flux is adopted due to flare events in this paper. However, the influence of time-dependent enhancements of UV flux on life or chemistry needs to be compared with the continuum UV enhancements. Through the simulation of phenomena such as solar activity, Ranjan et al.⁶⁰ found that secular time-dependent variations in the UV band have little influence on prebiotic chemistry, but they also suggested caution when extrapolating from high-fluence regimes to natural conditions. By modeling flares via pulsed UV radiation, microorganisms can tolerate high fluences of UV radiation in quantities, and at even shorter wavelengths than not experienced by microorganisms on present-day Earth.⁶¹ Thus, our assumption of an averaged UV flux is reasonable. Of course, more quantitative studies on the influence of time-dependent UV radiation on prebiotic chemistry would be preferred to refine the average assumption.

To accurately model or determine the UV radiation of stars, we need more NUV observations of various stars, especially young stars. In the quiescent stage, a survey including a large sample of stars is necessary to characterize the NUV radiation correlated with different stellar parameters, e.g., rotation period, age, metallicity, and effective temperature. Secular monitoring like *Kepler* and *TESS* would also be beneficial for characterizing the CFFD of flaring stars. Additionally, time-series observations or spectra during stellar flare events are crucial for understanding the physical processes and refining the SED model of flares.

Astrobiology experiments to explore the influence of UV flux on prebiotic chemistry are also crucial to determine the limits of UV radiation. UV radiation has both beneficial and detrimental effects on the accumulation of biological macromolecules such as RNA precursors. Extreme UV radiation can destroy prebiotic chemistry. However, the formation of life is a process of selective evolution over

long periods. Certain mechanisms protect these biomacromolecules, ensuring their survival at specific rates and probabilities, either in particular locations or within specific environments. Studying the shielding mechanisms^{48,62} in different environments can help refine the UV requirements for abiogenesis. Furthermore, testing the amount of cumulative products over a longer timescale under a wide range of UV radiation levels is critical for habitability studies. The quantitative assessment of the effects of UV radiation on the origin of life remains an open issue, requiring more data and interdisciplinary collaborations.

After the origin of life, many other aspects can also influence the sustenance of life. For example, the synthesis of genetic molecules is influenced by various factors. X-rays, coronal mass ejections (CMEs)^{63–65}, and stellar energetic particles (SEPs)^{66,67} can all cause water loss and affect planetary habitability via chemistry. Optimistically, when life exists on a planet, it can resist high UV radiation through mechanisms such as clumping and biofilm formation.⁴³ Therefore, further laboratory research is needed to study how microbes, such as *Deinococcus radiodurans*²¹ and tardigrade, perform in extreme UV environments to determine the upper limit of UV radiation for sustaining life.

CONCLUSION

Traditional habitable zones for liquid water are widely accepted for detecting habitable planets, while the UV radiation is considered by a lot of works to show its importance for life origins via prebiotic chemistry. Adopting the NUV (200–280 nm) requirements from previous experimental requirements of abiogenesis, and considering the effects on chemical reaction rate at different temperatures, we constrain the inner boundary of UV-HZ naturally. After correcting the quiescent stellar NUV radiation for young stars (~ 1 Gyr), based on the observation from GALEX, the UV-HZ can overlap with the LW-HZ in a narrow region for low mass stars. However, planets around these low-mass stars can hardly be located in the overlapped regions. To calculate the UV enhancement due to flares, we construct an SED model for flares and adopt an empirical model of CFFD correlated with different stars. We find that flaring stars can tolerate both LW-HZ and UV-HZ in the same region, much wider than the quiescent low mass stars. Therefore, the flaring low-mass stars can sustain the habitability of planets in the overlapped HZ. Specifically, we investigate nine Kepler flaring stars and refine their LW-HZ and UV-HZ, according to the observed CFFD. One rocky planet (KOI-8012.01) and two super-Earths (KOI-8047.01 and KOI-7703.01) are located within both habitable zones, avoiding the erosion of ozone in the atmosphere. The other three planets, i.e., Kepler-1540 b, Kepler-438 b, and Kepler-155 c, deserve further investigation for the surface temperature to assess their habitability. Our work provides a positive perspective on searching for habitable planets and potential life around flaring low-mass stars.

RESOURCE AVAILABILITY

Lead contact

Dong-Yang Gao: <https://orcid.org/0000-0001-6643-2138>; Hui-Gen Liu: <https://orcid.org/0000-0001-5162-1753>; Ming Yang: <https://orcid.org/0000-0002-6926-2872>; Ji-Lin Zhou: <https://orcid.org/0000-0003-1680-2940>.

Data and Code Availability

All data needed to evaluate the conclusions in the paper are present in the paper and/or the Supplemental Information. Additional data and code related to this paper are available from the lead contact upon request.

ACKNOWLEDGMENTS

These results are based on observations obtained with *Kepler*. We are grateful to the [Lightkurve](#)⁶⁸ for the valuable assistance in gathering our *Kepler* data. We thank Song Wang, Xue Li, and Jia-Hui Wang from the National Astronomical Observatories, Chinese Academy of Sciences, for their helpful discussions on stellar NUV radiation and stellar ages. We thank National Key R&D Program of China (No. 2024YFA1611801), National Natural Science Foundation of China (No. 12150009), China Manned Space Project (No. CMS-CSST-2025-A16), the Instrument Education Funds of Shandong University (No. yr20240205), the Civil Aerospace Technology Research Project (No. D010102), Fundamental and Interdisciplinary Disciplines Breakthrough Plan of the Ministry of Education of China (JYB2025XDXM105), and the Shanghai Municipal Education Commission's Artificial Intelligence Innovation Program for Empowering Discipline Development and Reforming Research Paradigms.

AUTHOR CONTRIBUTIONS

H.-G.L. proposed and designed this study. D.-Y.G., H.-G.L., and M.Y. investigated the observation data and pertinent literature. D.-Y.G. conducted the calculations and analysis. J.-L. Z. provides key suggestions on this work. All authors discussed the results and reviewed the manuscript.

DECLARATION OF INTERESTS

The authors declare no competing interests.

SUPPLEMENTAL INFORMATION

Supplemental Text, Figures S1 to S11, Tables S1 to S4, Supplemental References S1-S32.

REFERENCES

1. Borucki, W. J. (2016). KEPLER Mission: development and overview. Reports on Progress in Physics **79**: 036901. DOI: [10.1088/0034-4885/79/3/036901](https://doi.org/10.1088/0034-4885/79/3/036901).
2. Huang, S.-S. (1959). The Problem of Life in the Universe and the Mode of Star Formation. Publications of the Astronomical Society of the Pacific **71**: 421. DOI: [10.1086/127417](https://doi.org/10.1086/127417).
3. Kopparapu, R. K., Ramirez, R., Kasting, J. F., et al. (2013). Habitable Zones around Main-sequence Stars: New Estimates. The Astrophysical Journal **765**: 131. DOI: [10.1088/0004-637X/765/2/131](https://doi.org/10.1088/0004-637X/765/2/131).
4. Kopparapu, R. K., Hébrard, E., Belikov, R., et al. (2018). Exoplanet Classification and Yield Estimates for Direct Imaging Missions. The Astrophysical Journal **856**: 122. DOI: [10.3847/1538-4357/aab205](https://doi.org/10.3847/1538-4357/aab205).
5. Hill, M. L., Bott, K., Dalba, P. A., et al. (2023). A Catalog of Habitable Zone Exoplanets. The Astronomical Journal **165**: 34. DOI: [10.3847/1538-3881/aca1c0](https://doi.org/10.3847/1538-3881/aca1c0).

6. Kopparapu, R. K., Ramirez, R. M., SchottelKotte, J., et al. (2014). Habitable Zones around Main-sequence Stars: Dependence on Planetary Mass. *The Astrophysical Journal Letters* **787**: L29. DOI: [10.1088/2041-8205/787/2/L29](https://doi.org/10.1088/2041-8205/787/2/L29).
7. Cockell, C. S. (1999). Carbon Biochemistry and the Ultraviolet Radiation Environments of F, G, and K Main Sequence Stars. *Icarus* **141**: 399–407. DOI: [10.1006/icar.1999.6167](https://doi.org/10.1006/icar.1999.6167).
8. Buccino, A. P., Lemarchand, G. A., and Mauas, P. J. D. (2006). Ultraviolet radiation constraints around the circumstellar habitable zones. *Icarus* **183**: 491–503. DOI: [10.1016/j.icarus.2006.03.007](https://doi.org/10.1016/j.icarus.2006.03.007).
9. Xu, J., Ritson, D. J., Ranjan, S., et al. (2018). Photochemical reductive homologation of hydrogen cyanide using sulfite and ferrocyanide. *Chem. Commun.* **54**: (44), 5566–5569. DOI: [10.1039/C8CC01499J](https://doi.org/10.1039/C8CC01499J).
10. Rimmer, P. B., Xu, J., Thompson, S. J., et al. (2018). The origin of RNA precursors on exoplanets. *Science Advances* **4**: eaar3302. DOI: [10.1126/sciadv.aar3302](https://doi.org/10.1126/sciadv.aar3302).
11. Arrhenius, S. (1900). Les oscillations séculaires de la température á la surface du globe terrestre. *Ciel et Terre* **20**: 389–396.
12. Guo, J., Zhang, F., Zhang, X., et al. (2010). Habitable zones and UV habitable zones around host stars. **325**: 25–30. DOI: [10.1007/s10509-009-0173-9](https://doi.org/10.1007/s10509-009-0173-9).
13. Spinelli, R., Borsa, F., Ghirlanda, G., et al. (2023). The ultraviolet habitable zone of exoplanets. *Monthly Notices of the Royal Astronomical Society* **522**: 1411–1418. DOI: [10.1093/mnras/stad928](https://doi.org/10.1093/mnras/stad928).
14. Pettersen, B. R. (1989). A Review of Stellar Flares and Their Characteristics. *Solar Physics* **121**: 299–312. DOI: [10.1007/BF00161702](https://doi.org/10.1007/BF00161702).
15. Benz, A. O. and Güdel, M. (2010). Physical Processes in Magnetically Driven Flares on the Sun, Stars, and Young Stellar Objects. *Annual Review of Astronomy and Astrophysics* **48**: 241–287. DOI: [10.1146/annurev-astro-082708-101757](https://doi.org/10.1146/annurev-astro-082708-101757).
16. Shibata, K. and Takasao, S. (2016). “Fractal Reconnection in Solar and Stellar Environments”. *Magnetic Reconnection: Concepts and Applications*. Ed. by W. Gonzalez and E. Parker. Vol. 427. *Astrophysics and Space Science Library*, 373. DOI: [10.1007/978-3-319-26432-5_10](https://doi.org/10.1007/978-3-319-26432-5_10).
17. Günther, M. N., Zhan, Z., Seager, S., et al. (2020). Stellar Flares from the First TESS Data Release: Exploring a New Sample of M Dwarfs. *The Astronomical Journal* **159**: 60. DOI: [10.3847/1538-3881/ab5d3a](https://doi.org/10.3847/1538-3881/ab5d3a).
18. Gao, D.-Y., Liu, H.-G., Yang, M., et al. (2022). Correcting Stellar Flare Frequency Distributions Detected by TESS and Kepler. *The Astronomical Journal* **164**: 213. DOI: [10.3847/1538-3881/ac937e](https://doi.org/10.3847/1538-3881/ac937e).
19. Jackman, J. A. G., Shkolnik, E. L., Million, C., et al. (2023). Extending optical flare models to the UV: results from comparing of TESS and GALEX flare observations for

- M Dwarfs. *Monthly Notices of the Royal Astronomical Society* **519**: 3564–3583. DOI: [10.1093/mnras/stac3135](https://doi.org/10.1093/mnras/stac3135).
20. Youngblood, A., France, K., Loyd, R. O. P., et al. (2017). The MUSCLES Treasury Survey. IV. Scaling Relations for Ultraviolet, Ca II K, and Energetic Particle Fluxes from M Dwarfs. *The Astrophysical Journal* **843**: 31. DOI: [10.3847/1538-4357/aa76dd](https://doi.org/10.3847/1538-4357/aa76dd).
 21. Tilley, M. A., Segura, A., Meadows, V., et al. (2019). Modeling Repeated M Dwarf Flaring at an Earth-like Planet in the Habitable Zone: Atmospheric Effects for an Unmagnetized Planet. *Astrobiology* **19**: 64–86. DOI: [10.1089/ast.2017.1794](https://doi.org/10.1089/ast.2017.1794).
 22. Jackman, J. A. G., Wheatley, P. J., Acton, J. S., et al. (2021). Stellar flares detected with the Next Generation Transit Survey. *Monthly Notices of the Royal Astronomical Society* **504**: 3246–3264. DOI: [10.1093/mnras/stab979](https://doi.org/10.1093/mnras/stab979).
 23. Yang, H. and Liu, J. (2019). The Flare Catalog and the Flare Activity in the Kepler Mission. *The Astrophysical Journal Supplement Series* **241**: 29. DOI: [10.3847/1538-4365/ab0d28](https://doi.org/10.3847/1538-4365/ab0d28).
 24. Brasseur, C. E., Osten, R. A., Tristan, I. I., et al. (2023). Constraints on Stellar Flare Energy Ratios in the NUV and Optical from a Multiwavelength Study of GALEX and Kepler Flare Stars. *The Astrophysical Journal* **944**: 5. DOI: [10.3847/1538-4357/acab59](https://doi.org/10.3847/1538-4357/acab59).
 25. Kowalski, A. F. (2022). Near-Ultraviolet Continuum Modeling of the 1985 April 12 Great Flare of AD Leo. *Frontiers in Astronomy and Space Sciences* **9**: 351. DOI: [10.3389/fspas.2022.1034458](https://doi.org/10.3389/fspas.2022.1034458).
 26. Loyd, R. O. P., Shkolnik, E. L., Schneider, A. C., et al. (2018). HAZMAT. IV. Flares and Superflares on Young M Stars in the Far Ultraviolet. *The Astrophysical Journal* **867**: 70. DOI: [10.3847/1538-4357/aae2ae](https://doi.org/10.3847/1538-4357/aae2ae).
 27. Li, X., Wang, S., Han, H., et al. (2024). Ultraviolet and Chromospheric Activity and Habitability of M Stars. *The Astrophysical Journal* **966**: 69. DOI: [10.3847/1538-4357/ad3038](https://doi.org/10.3847/1538-4357/ad3038).
 28. Watanabe, K., Kitagawa, J., and Masuda, S. (2017). Characteristics that Produce White-light Enhancements in Solar Flares Observed by Hinode/SOT. *The Astrophysical Journal* **850**: 204. DOI: [10.3847/1538-4357/aa9659](https://doi.org/10.3847/1538-4357/aa9659).
 29. Watanabe, K. and Imada, S. (2020). White-light Emission and Chromospheric Response by an X1.8-class Flare on 2012 October 23. *The Astrophysical Journal* **891**: 88. DOI: [10.3847/1538-4357/ab711b](https://doi.org/10.3847/1538-4357/ab711b).
 30. Okamoto, S., Notsu, Y., Maehara, H., et al. (2021). Statistical Properties of Superflares on Solar-type Stars: Results Using All of the Kepler Primary Mission Data. *The Astrophysical Journal* **906**: 72. DOI: [10.3847/1538-4357/abc8f5](https://doi.org/10.3847/1538-4357/abc8f5).
 31. Kowalski, A. F. (2023). Bridging High-density Electron Beam Coronal Transport and Deep Chromospheric Heating in Stellar Flares. *The Astrophysical Journal Letters* **943**: L23. DOI: [10.3847/2041-8213/acb144](https://doi.org/10.3847/2041-8213/acb144).

32. Kretzschmar, M. (2011). The Sun as a star: observations of white-light flares. *Astronomy & Astrophysics* **530**: A84. DOI: [10.1051/0004-6361/201015930](https://doi.org/10.1051/0004-6361/201015930).
33. Kleint, L., Heinzel, P., Judge, P., et al. (2016). Continuum Enhancements in the Ultraviolet, the Visible and the Infrared during the X1 Flare on 2014 March 29. *The Astrophysical Journal* **816**: 88. DOI: [10.3847/0004-637X/816/2/88](https://doi.org/10.3847/0004-637X/816/2/88).
34. Kowalski, A. F., Wisniewski, J. P., Hawley, S. L., et al. (2019). The Near-ultraviolet Continuum Radiation in the Impulsive Phase of HF/GF-type dMe Flares. I. Data. *The Astrophysical Journal* **871**: 167. DOI: [10.3847/1538-4357/aaf058](https://doi.org/10.3847/1538-4357/aaf058).
35. France, K., Loyd, R. O. P., Youngblood, A., et al. (2016). The MUSCLES Treasury Survey. I. Motivation and Overview. *The Astrophysical Journal* **820**: 89. DOI: [10.3847/0004-637X/820/2/89](https://doi.org/10.3847/0004-637X/820/2/89).
36. Richey-Yowell, T., Shkolnik, E. L., Loyd, R. O. P., et al. (2022). HAZMAT. VIII. A Spectroscopic Analysis of the Ultraviolet Evolution of K Stars: Additional Evidence for K Dwarf Rotational Stalling in the First Gigayear. *The Astrophysical Journal* **929**: 169. DOI: [10.3847/1538-4357/ac5f48](https://doi.org/10.3847/1538-4357/ac5f48).
37. Osten, R. A. and Wolk, S. J. (2015). Connecting Flares and Transient Mass-loss Events in Magnetically Active Stars. *The Astrophysical Journal* **809**: 79. DOI: [10.1088/0004-637X/809/1/79](https://doi.org/10.1088/0004-637X/809/1/79).
38. Kowalski, A. F., Allred, J. C., Uitenbroek, H., et al. (2017). Hydrogen Balmer Line Broadening in Solar and Stellar Flares. *The Astrophysical Journal* **837**: 125. DOI: [10.3847/1538-4357/aa603e](https://doi.org/10.3847/1538-4357/aa603e).
39. Shibata, K. and Magara, T. (2011). Solar Flares: Magnetohydrodynamic Processes. *Living Reviews in Solar Physics* **8**: 6. DOI: [10.12942/lrsp-2011-6](https://doi.org/10.12942/lrsp-2011-6).
40. Tu, Z.-L., Yang, M., Zhang, Z. J., et al. (2020). Superflares on Solar-type Stars from the First Year Observation of TESS. *The Astrophysical Journal* **890**: 46. DOI: [10.3847/1538-4357/ab6606](https://doi.org/10.3847/1538-4357/ab6606).
41. Popp, M., Schmidt, H., and Marotzke, J. (2016). Transition to a Moist Greenhouse with CO₂ and solar forcing. *Nature Communications* **7**: 10627. DOI: [10.1038/ncomms10627](https://doi.org/10.1038/ncomms10627).
42. Ranjan, S., Wordsworth, R., and Sasselov, D. D. (2017). The Surface UV Environment on Planets Orbiting M Dwarfs: Implications for Prebiotic Chemistry and the Need for Experimental Follow-up. *The Astrophysical Journal* **843**: 110. DOI: [10.3847/1538-4357/aa773e](https://doi.org/10.3847/1538-4357/aa773e).
43. Abrevaya, X. C., Leitzinger, M., Oppezzo, O. J., et al. (2020). The UV surface habitability of Proxima b: first experiments revealing probable life survival to stellar flares. *Monthly Notices of the Royal Astronomical Society* **494**: L69–L74. DOI: [10.1093/mnrasl/slaa037](https://doi.org/10.1093/mnrasl/slaa037).
44. Loyd, R. O. P., France, K., Youngblood, A., et al. (2016). The MUSCLES Treasury Survey. III. X-Ray to Infrared Spectra of 11 M and K Stars Hosting Planets. *The Astrophysical Journal* **824**: 102. DOI: [10.3847/0004-637X/824/2/102](https://doi.org/10.3847/0004-637X/824/2/102).

45. Wang, S., Li, X., Han, H., et al. (2024). Predicting Photospheric Ultraviolet Emission from Stellar Evolutionary Models. *The Astrophysical Journal* **976**: 43. DOI: [10.3847/1538-4357/ad87d0](https://doi.org/10.3847/1538-4357/ad87d0).
46. Segura, A., Walkowicz, L. M., Meadows, V., et al. (2010). The Effect of a Strong Stellar Flare on the Atmospheric Chemistry of an Earth-like Planet Orbiting an M Dwarf. *Astrobiology* **10**: 751–771. DOI: [10.1089/ast.2009.0376](https://doi.org/10.1089/ast.2009.0376).
47. Todd, Z. R., Szostak, J. W., and Sasselov, D. D. (2021). Shielding from UV Photodamage: Implications for Surficial Origins of Life Chemistry on the Early Earth. *ACS Earth and Space Chemistry* **5**: 239–246. DOI: [10.1021/acsearthspacechem.0c00270](https://doi.org/10.1021/acsearthspacechem.0c00270).
48. Ranjan, S., Kufner, C. L., Lozano, G. G., et al. (2022). UV Transmission in Natural Waters on Prebiotic Earth. *Astrobiology* **22**: 242–262. DOI: [10.1089/ast.2020.2422](https://doi.org/10.1089/ast.2020.2422).
49. Mojzsis, S. J., Arrhenius, G., McKeegan, K. D., et al. (1996). Evidence for life on Earth before 3,800 million years ago. *Nature* **384**: 55–59. DOI: [10.1038/384055a0](https://doi.org/10.1038/384055a0).
50. Dodd, M. S., Papineau, D., Grenne, T., et al. (2017). Evidence for early life in Earth’s oldest hydrothermal vent precipitates. **543**: 60–64. DOI: [10.1038/nature21377](https://doi.org/10.1038/nature21377).
51. Cavalazzi, B., Lemelle, L., Simionovici, A., et al. (2021). Cellular remains in a 3.42-billion-year-old seafloor hydrothermal environment. *Science Advances* **7**: eabf3963. DOI: [10.1126/sciadv.abf3963](https://doi.org/10.1126/sciadv.abf3963).
52. Shkolnik, E. L. and Barman, T. S. (2014). HAZMAT. I. The Evolution of Far-UV and Near-UV Emission from Early M Stars. *The Astronomical Journal* **148**: 64. DOI: [10.1088/0004-6256/148/4/64](https://doi.org/10.1088/0004-6256/148/4/64).
53. Baraffe, I., Homeier, D., Allard, F., et al. (2015). New evolutionary models for pre-main sequence and main sequence low-mass stars down to the hydrogen-burning limit. *Astronomy & Astrophysics* **577**: A42. DOI: [10.1051/0004-6361/201425481](https://doi.org/10.1051/0004-6361/201425481).
54. Willmer, C. N. A. (2018). The Absolute Magnitude of the Sun in Several Filters. *The Astrophysical Journal Supplement Series* **236**: 47. DOI: [10.3847/1538-4365/aabfdf](https://doi.org/10.3847/1538-4365/aabfdf).
55. Li, X., Wang, S., Ma, J., et al. (2025). Evolution of Stellar Activity and Habitable Zone. I. Ultraviolet Emission of Dwarfs in Open Clusters and Field Stars. *The Astrophysical Journal Supplement Series* **281**: 13. DOI: [10.3847/1538-4365/ae08a9](https://doi.org/10.3847/1538-4365/ae08a9).
56. Thompson, S. E., Coughlin, J. L., Hoffman, K., et al. (2018). Planetary Candidates Observed by Kepler. VIII. A Fully Automated Catalog with Measured Completeness and Reliability Based on Data Release 25. *The Astrophysical Journal Supplement Series* **235**: 38. DOI: [10.3847/1538-4365/aab4f9](https://doi.org/10.3847/1538-4365/aab4f9).
57. Kempton, E. M. .-, Bean, J. L., Louie, D. R., et al. (2018). A Framework for Prioritizing the TESS Planetary Candidates Most Amenable to Atmospheric Characterization. *Publications of the Astronomical Society of the Pacific* **130**: 114401. DOI: [10.1088/1538-3873/aadf6f](https://doi.org/10.1088/1538-3873/aadf6f).

58. Hall, C., Stancil, P. C., Terry, J. P., et al. (2023). A New Definition of Exoplanet Habitability: Introducing the Photosynthetic Habitable Zone. *The Astrophysical Journal Letters* **948**: L26. DOI: [10.3847/2041-8213/acccfb](https://doi.org/10.3847/2041-8213/acccfb).
59. Riihelä, A., Bright, R. M., and Anttila, K. (2021). Recent strengthening of snow and ice albedo feedback driven by Antarctic sea-ice loss. *Nature Geoscience* **14**: 832–836. DOI: [10.1038/s41561-021-00841-x](https://doi.org/10.1038/s41561-021-00841-x).
60. Ranjan, S. and Sasselov, D. D. (2016). Influence of the UV Environment on the Synthesis of Prebiotic Molecules. *Astrobiology* **16**: 68–88. DOI: [10.1089/ast.2015.1359](https://doi.org/10.1089/ast.2015.1359).
61. Abrevaya, X. C., Odert, P., Leitzinger, M., et al. (2025). The EXO-UV Program: Latest Advances of Experimental Studies to Investigate the Biological Impact of UV Radiation on Exoplanets. *Solar System Research* **59**: 72. DOI: [10.1134/S0038094624602019](https://doi.org/10.1134/S0038094624602019).
62. Sajeev, Y. (2023). Prebiotic chemical origin of biomolecular complementarity. *Communications Chemistry* **6**: 259. DOI: [10.1038/s42004-023-01060-8](https://doi.org/10.1038/s42004-023-01060-8).
63. Kay, C., Opher, M., and Kornbleuth, M. (2016). Probability of CME Impact on Exoplanets Orbiting M Dwarfs and Solar-like Stars. *The Astrophysical Journal* **826**: 195. DOI: [10.3847/0004-637X/826/2/195](https://doi.org/10.3847/0004-637X/826/2/195).
64. Khodachenko, M. L., Ribas, I., Lammer, H., et al. (2007). Coronal Mass Ejection (CME) Activity of Low Mass M Stars as An Important Factor for The Habitability of Terrestrial Exoplanets. I. CME Impact on Expected Magnetospheres of Earth-Like Exoplanets in Close-In Habitable Zones. *Astrobiology* **7**: 167–184. DOI: [10.1089/ast.2006.0127](https://doi.org/10.1089/ast.2006.0127).
65. Peña-Moñino, L., Pérez-Torres, M., Varela, J., et al. (2024). Magnetohydrodynamic simulations of the space weather in Proxima b: Habitability conditions and radio emission. *Astronomy & Astrophysics* **688**: A138. DOI: [10.1051/0004-6361/202349042](https://doi.org/10.1051/0004-6361/202349042).
66. Yamashiki, Y. A., Maehara, H., Airapetian, V., et al. (2019). Impact of Stellar Superflares on Planetary Habitability. *The Astrophysical Journal* **881**: 114. DOI: [10.3847/1538-4357/ab2a71](https://doi.org/10.3847/1538-4357/ab2a71).
67. Hu, J., Airapetian, V. S., Li, G., et al. (2022). Extreme energetic particle events by superflare-associated CMEs from solar-like stars. *Science Advances* **8**: eabi9743. DOI: [10.1126/sciadv.abi9743](https://doi.org/10.1126/sciadv.abi9743).
68. Lightkurve Collaboration, Cardoso, J. V. d. M., Hedges, C., et al. (2018). Lightkurve: Kepler and TESS time series analysis in Python. *Astrophysics Source Code Library*, record ascl:1812.013.

Supplemental Information for Flare-driven habitability: Expanding life's potential around low-mass stars

Dong-Yang Gao^{1,2,6}, Hui-Gen Liu^{1,4,6,*}, Ming Yang^{3,5,6,*}, and Ji-Lin Zhou^{1,4}

⁶These authors contributed equally to this work.

*Corresponding author. Email: huigen@nju.edu.cn (H.-G.L.); myang@tongji.edu.cn (M.Y.)

This PDF file includes:

Supplemental Text

Figures S1 to S11

Tables S1 to S4

Supplemental References S1-S32

Supplemental Text

Average luminosity of flaring stars

Flare spectral energy distribution

In the SED model, flare radiation in the UV band (0.100 to 0.365 μm) follows a power-law continuum superimposed with a hot-blackbody spectrum, while the white-light band follows a 9,000 K hot-blackbody model. A Balmer jump separates the two regions. This model is based on previous studies,^{S1-S3} and has integrated emission-line contributions into the continuum. The detailed flare spectral energy distribution model of the flare is shown in Equation (1) in the main paper.

We derived the parameters f_b and γ of the flare SED model based on the spectral observations of flares on AD Leo and the simulated flare SED of the G-type star. The fitted results are shown in Table S1 and illustrated in Figure S1A. Adopting a linear correlation assumption, as T_{eff} ranges from 3,400 K to 6,000 K, f_b decreases from 1.013 to 0.011, while γ varies from -0.500 to 1.032. Figure S1B displays several flare SED models. Note that this study primarily investigates the effects of flares on the habitable zone across different spectral types, where f_b and γ are indicative of characteristics of certain spectral types rather than individual stars.

To validate the flare SED model, we compared the calculated NUV flux with the observation results. The observed spectra are chosen as the peak flare spectra on AD Leo at 915 s from Segura et al.^{S4} Figure S2 illustrates the comparison result. The total energy of the SED model is only 7% less than the observed spectral energy in the UVC band (0.2 - 0.28 μm). Furthermore, we estimated the total energy correction factor for M stars, i.e., the flare energy ratio between the SED model and the 9,000K hot-blackbody spectrum. Our results are consistent with the estimated values of different previous works in various UV bands, as evidenced in Table S2. Therefore, the continuum flare SED model in this paper is suitable. Since there is lack of observed SED in the NUV band for K stars, it is difficult to validate the SED model for K stars. However, the flare enhancement in the NUV band usually contributes less for the G and K stars; therefore, we linearly interpolate the SED model for the K star.

Table S1. The spectrum and fitted values of f_b and γ in the flare SED model.

Spectral Type	spectrum	f_b	γ
M-type star	AD Leo: flare spectrum near H γ peak ^a	0.486 \pm 0.190	0.829 \pm 0.470
	800 s	0.277 \pm 0.131	0.072 \pm 0.487
	915 s (Peak) 1,038 s	0.206 \pm 0.141	-0.140 \pm 0.700
AD Leo: flare spectrum at U band peak ^b	Observation	1.013 \pm 0.159	-0.052 \pm 0.133
	Model	0.884 \pm 0.331	-0.014 \pm 0.240
G-type star	UV flare photometry ^c	1.0 \pm 0.4	-0.5 $^{+0.2}_{-0.4}$
	Hot-BlackBody Model	0.011 \pm 0.001	1.032 \pm 0.118
	9,000 K 10,000 K	0.251 \pm 0.009	0.623 \pm 0.048

^a Segura et al.^{S4} provide synthetic flare spectra near the peak of the H γ line around 915 seconds.

^b Kowalski^{S5} provides a synthetic flare spectrum and continuum observations at the U band peak around 542 seconds.

^c Fleming et al.^{S6} provide 21 flare events observed on GJ 65 in both GALEX FUV ($\lambda_{\text{eff}} = 0.1539 \mu\text{m}$, $\Delta\lambda = 0.1344 - 0.1786 \mu\text{m}$) and NUV ($\lambda_{\text{eff}} = 0.2316 \mu\text{m}$, $\Delta\lambda = 0.1771 - 0.2831 \mu\text{m}$) bands. Fleming et al.^{S6} provide the clues of γ , which is used to determine f_b by incorporating the Energy Correction Factor (ECF) of 2.7 ± 0.6 from Jackman et al.^{S3}

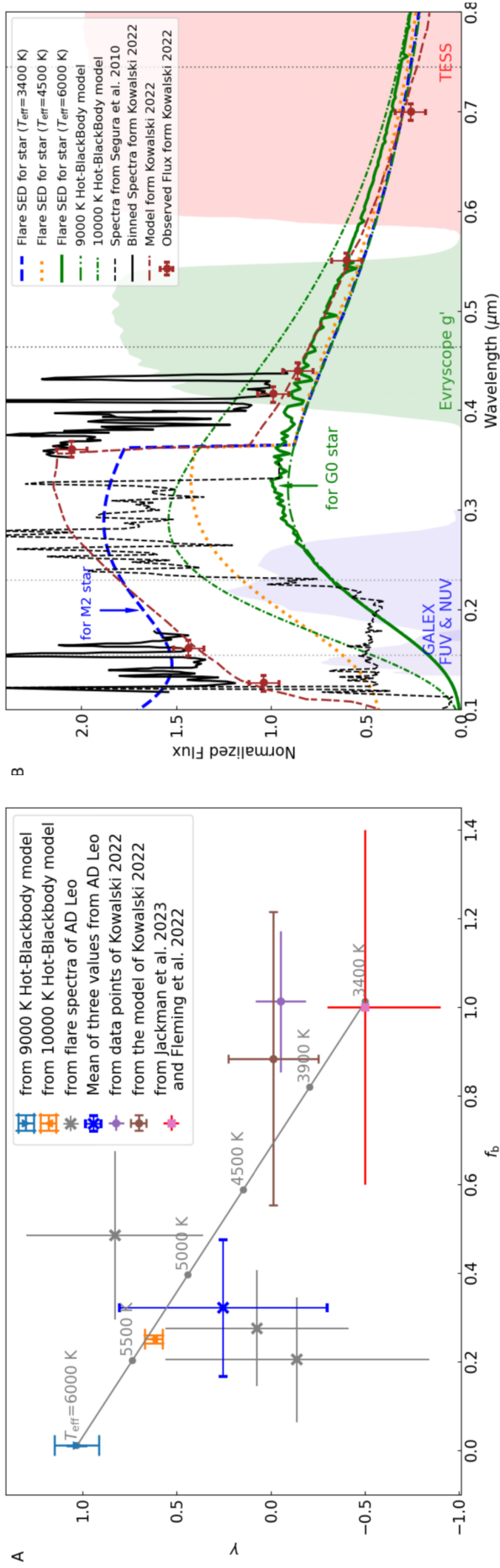


Figure S1. (A) Parameters of flare SED. The parameters are derived from flare spectra and models in Table S1. The gray line represents the linearly scaled model for the flare SED with varying stellar effective temperature (T_{eff}). **(B) Flare SED for different stars.** The solid, dotted, and dashed lines in various colors represent flare SED models for different stars with $T_{\text{eff}} = 6,000$ K, 4,500 K, and 3,400 K, respectively. The black solid line represents the adjusted “great flare” spectra of AD Leo, with plus symbols marking the data from wavelength-binned observed continuum fluxes by Kowalski.^{S5} The red long-short-dashed line is the best fit using a two-component radiative-hydrodynamic model from the same study. The gray dashed line is the “great flare” spectra from Segura et al.^{S4} The green long-dash-dotted and short-dash-dotted lines show the 9,000 and 10,000 K hot-blackbody model, respectively. Colored backgrounds show the relative band-passes of different filters, with gray vertical dotted lines marking the mean wavelengths for GALEX FUV band (0.155 μm), GALEX NUV band (0.230 μm), Evryscope g' band (0.464 μm), and TESS band (0.745 μm).

Table S2. Comparison of the flare SED model with previous models and observations for M stars.

Parameters	Previous Work	This Work
ECF^a in NUV	2.7 ± 0.6^{S3} 3.86^{S7} $2-3^{S8}$	2.87
ECF in FUV	6.5 ± 0.7^{S3} 12.6^{S7}	9.38
F_{FUV}/F_{NUV}^b	0.85 ± 0.52^{S6} $0.5-2^{S7}$	0.85
$F_{0.2 \mu m}/F_{0.28 \mu m}^c$	1.3^{S5} $\sim 0.9^{S4}$	1.2
$F_{0.464 \mu m, g'}/F_{0.745 \mu m, TESS}^d$	2.78 ± 0.1^{S9}	2.65

^a Energy Correction Factor (ECF) under the 9,000 K hot-blackbody assumption.

^b Flux ratio derived by GALEX FUV and NUV bands, including 21 flare events from GJ 65^{S6} and 182 events from primarily M-type stars.^{S7}

^c Flux ratio derived from the SED models of Kowalski^{S5} and Segura et al.^{S4} for the “great flare” of AD Leo.

^d Flux ratio derived from multiple superflares observed by Evryscope and TESS, detailed in Howard et al.^{S9}

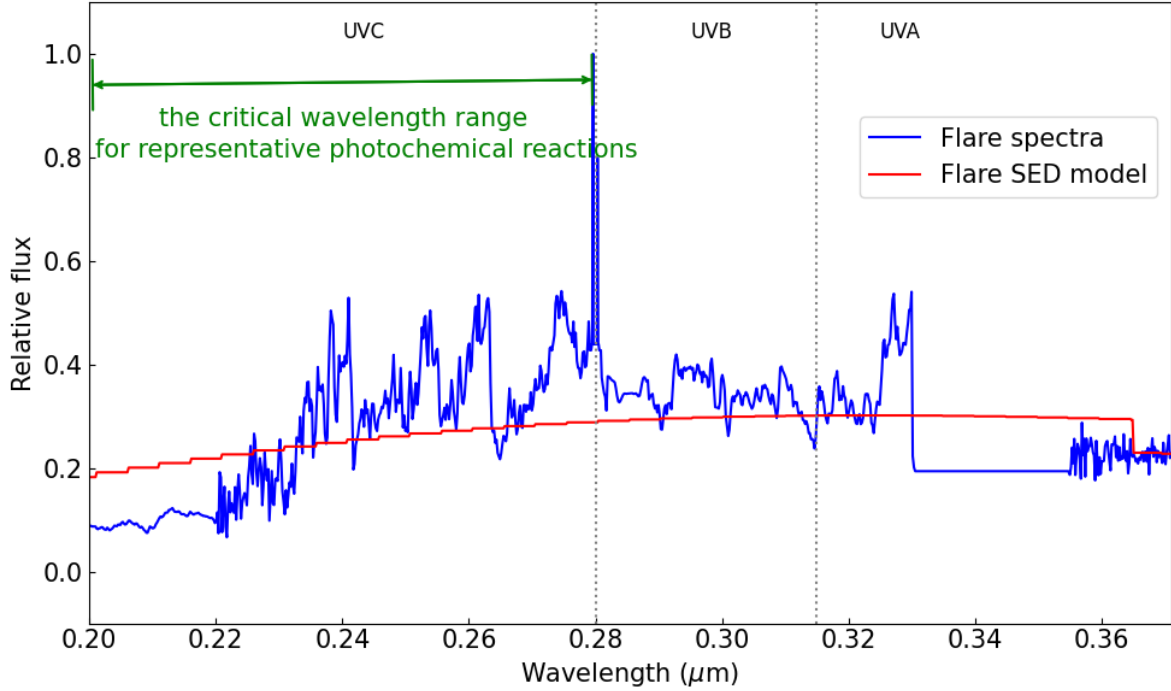


Figure S2. Comparison of observed flare spectrum with the SED model. The blue line represents the multi-band composite spectrum synthesized by Segura et al.^{S4} at 915 s. The red line represents the SED model described in the main paper. Grey vertical dotted lines demarcate the boundaries between UVA and UVB (0.315 μm), UVB and UVC (0.28 μm). The green horizontal arrow highlights the NUV wavelength range (0.20–0.28 μm), which is vital for photochemical reactions.^{S10} In this range, the flux ratio of the flare spectra to the SED model is approximately 1.07.

Quiescent NUV radiation correction based on observations

To accurately estimate the NUV emission of stars in the quiescent state, we used the ratio of photospheric emission to total observed emission via GALEX NUV band^{S11} (see Table S4). Also, to match the general case used in this paper (i.e., the stellar age is 1.0 Gyr, and the metallicity [Fe/H] is 0), we used the age information provided by Wang J. H.^{S12} and the [Fe/H] parameter provided by Wang S.^{S11}. We found that the median values of the full sample and the filtered sample (Age: 0.6–1.4 Gyr, [Fe/H] \sim -0.2–0.2) were close (see Figure S3). Due to the lack of stars with temperatures below 4,000 K in the filtered sample, we adopted the statistical median values of the full sample in the NUV flux correction.

Enhancement of stellar luminosity caused by flares

The cumulative flare frequency distribution (CFFD), denoted by ν , can be described as

$$\nu = k_c E^{\alpha_c} \quad (\text{S1})$$

or

$$\log_{10}(\nu) = \beta_c + \alpha_c \times \log_{10}(E), \quad (\text{S2})$$

where $\beta_c = \log_{10}(k_c)$. The occurrence frequency of flares with energies between E and $E + dE$ is given by

$$d\nu(E) = k_c \alpha_c E^{(\alpha_c - 1)} dE. \quad (\text{S3})$$

If the unit of k_c is set as day^{-1} , then the total flare energy per day is

$$E_{\text{total}} = \int_{E_{\text{low}}}^{E_{\text{high}}} E d\nu(E) dE = \int_{E_{\text{low}}}^{E_{\text{high}}} k_c \alpha_c E^{\alpha_c} dE \quad (\text{S4})$$

$$= \begin{cases} \alpha_c 10^{\beta_c} \times (E_{\text{high}}^{(\alpha_c+1)} - E_{\text{low}}^{(\alpha_c+1)}) / (\alpha_c + 1), & \text{for } \alpha_c \neq -1 \\ \alpha_c 10^{\beta_c} \times \ln(E_{\text{high}}/E_{\text{low}}), & \text{for } \alpha_c = -1 \end{cases} \quad (\text{S5})$$

where E_{low} and E_{high} are the lower and upper energy limits considered in the calculation, respectively. The energy range for detected solar and stellar flares spans from 10^{28} to 10^{38} erg. [S13–S16](#)

The averaged increase in stellar luminosity due to flares is:

$$L_{\text{flare}} = E_{\text{total}} / (1 \text{ day}) = E_{\text{total}} / (86400 \text{ s}). \quad (\text{S6})$$

Using the α_c and β_c values from our previous study, [S17](#) we obtained the distribution relationship of α_c and β_c with T_{eff} for stars ranging from M2 to G1 as follows:

$$\alpha_c = \begin{cases} 0.44(\pm 0.01) \times \frac{T_{\text{eff}}}{1000 \text{ K}} - 2.84(\pm 0.05), & \text{for } 3400 \text{ K} \leq T_{\text{eff}} < 5150 \text{ K} \\ -0.53(\pm 0.03) \times \frac{T_{\text{eff}}}{1000 \text{ K}} + 2.18(\pm 0.18), & \text{for } 5150 \text{ K} \leq T_{\text{eff}} \leq 5900 \text{ K} \end{cases} \quad (\text{S7})$$

$$\beta_c = -32.0 \times \alpha_c - 1.09 \times 10^{-7} (\pm 1.10 \times 10^{-4}) \times \frac{T_{\text{eff}}}{1000 \text{ K}} + 1.12(\pm 0.54). \quad (\text{S8})$$

In our previous study, which relied on the assumption of a 9,000 K hot-blackbody model, [S17](#) the contribution of UV radiation was underestimated. Adopting the validated SED model in the main paper, we can calculate a correction factor for the modeled flux in the NUV band, i.e.,

$$R_{\text{corrected}} = \frac{\int_{\text{bol}} F_{\lambda}(T_{\text{flare}}) d\lambda}{\int_{\text{bol}} B_{\lambda}(T_{\text{flare}}) d\lambda}, \quad (\text{S9})$$

where T_{flare} represents the flare temperature and is set to be 9,000 K, F_{λ} is the flare spectrum according to the flare SED model (Equation 1 in the main paper), and $B_{\lambda}(T_{\text{flare}})$ is the Planck function evaluated at the flare temperature. For instance, for the G-type star KOI-7703, $R_{\text{corrected}} = 1.14$; while for the M-type star Kepler-1512, $R_{\text{corrected}} = 1.87$.

After the correction of the flare energy, the slope of CFFD is unchanged (i.e., α_c remains constant), while β_c increases. The updated β'_c after correction can be described by the fitted parameter before correction:

$$\beta'_c = -\log_{10}(R_{\text{corrected}}) \times \alpha_c + \beta_c. \quad (\text{S10})$$

The empirical CFFDs of typical G, K, and M stars after correction are shown in Figure [S4](#). For most M-type flaring stars, we find $\alpha_c < -1$, indicating that low-energy flares contribute the majority of the total flare energy. On the contrary, for stars hotter than K5, we find $\alpha_c > -1$, indicating that high-energy flares are dominant. [S17–S20](#)

Due to the CFFD of different stars, the averaged enhancement of bolometric luminosity of a star due to flares (L_{flare}) can be obtained directly by Equation (S6). To estimate the averaged enhancement of UV luminosity, we need to combine the SED model to estimate the area of active regions during flares, A_{flare} . According to the following equation:

$$\frac{L_{\text{flare}}}{L_*} = \frac{A_{\text{flare}} \int_{\text{bol}} F_{\text{flare}}(\lambda) d\lambda}{\pi R_*^2 \int_{\text{bol}} S_*(\lambda) d\lambda}, \quad (\text{S11})$$

where $F_{\text{flare}}(\lambda)$ is the flare SED as defined in Equation (1) in the main paper, and $S_*(\lambda)$ is the stellar

spectra in quiescent stage after correction. Since we already know the values of both L_{flare} and the luminosity of star in quiescent stage L_* , we can calculate the dimensionless ratio:

$$\frac{A_{\text{flare}}}{\pi R_*^2} = \frac{\frac{L_{\text{flare}}}{L_*}}{\frac{\int_{\text{bol}} F_{\text{flare}}(\lambda) d\lambda}{\int_{\text{bol}} S_*(\lambda) d\lambda}}. \quad (\text{S12})$$

The bolometric integral of the spectra is integrated from 0.1 to 3 μm . Then we can estimate the average enhancement in the NUV band as follows by integration from 0.2 to 0.28 μm :

$$f_{\text{flare, NUV}} = \frac{A_{\text{flare}} \int_{\text{NUV}} F_{\text{flare}}(\lambda) d\lambda}{\pi R_*^2 \int_{\text{NUV}} S_*(\lambda) d\lambda}. \quad (\text{S13})$$

UV Habitable Zone of Flaring stars

Habitable zones around different types of flaring stars

We adopt our previous study^{S17} to describe the CFFD for different flaring stars with age ~ 1 Gyr. Based on 121 flaring star samples, including G, K, and M stars, we obtained consistent α with other research as shown in Figure S5. An empirical relationship between the CFFD and stellar effective temperature (T_{eff}) is achieved, as shown in Equation S7 and S8. The rotating period of the stars are between 1 and 5 day, which induced an age of around 0.1 to 3 Gyr via empirical gyrochronology isochrones.^{S14,S21} Furthermore, 57 (47%) of the 121 samples also have ages from FLAME (Final Luminosity Age Mass Estimator^{S22}) with 95% of them being older than 1 Gyr. Therefore, the correlations are adopted to represent the CFFD of stars around 1.0 Gyr old.

To estimate the stellar parameters around 1 Gyr, we use the stellar evolution model described by Baraffe et al.^{S23} The stellar masses are set between 1.1 and 0.3 solar masses to represent different G, M, and K stars, and we calculate their effective temperatures (T_{eff}) and radii (R_*) at 1 Gyr. The photospheric NUV flux is generated by the Phoenix model according to the stellar parameters ($[\text{Fe}/\text{H}]=0$). Then we do correction for quiescent NUV radiation by dividing the median value of the full sample in Figure S3. These parameters were subsequently utilized to calculate the inner boundary of the UV-HZ with flares for the general case. Considering the planetary atmosphere transmittance, ozone and oxygen are absent in the atmosphere of Archean Earth. Thus, we adopt the atmosphere transmittance as 0.84 for K and G stars (with effective temperatures $T_{\text{eff}} \geq 5,000$ K and masses $M_* \geq 0.84 M_{\odot}$), and 0.74 for cooler stars ($T_{\text{eff}} < 5,000$ K).^{S24} Figure S6 illustrates LW-HZ (green area) and UV-HZ (purple area) for flaring stars across various T_{eff} . For a better view, Figure 3 in the main paper illustrates the boundaries of the habitable zones both with and without flares for different stellar masses.

Habitable Zones around Kepler flaring hosts

For *Kepler* flaring stars, we fit the CFFD parameters α_{C} and β'_{C} for all nine stars, as shown in Table S3. The updated stellar and planetary parameters are presented in Table S4. We obtained their boundaries of the LW-HZs and the UV-HZs as shown in Table 1 in the main paper and Figure S7. Figure 5 in the main paper also illustrates these boundaries for a better view.

The requirements of observed CFFD for abiogenesis

For flaring stars, flares in certain bands are directly observed; thus, we can obtain the flare energy in such a band, rather than the total energy. To estimate the abiogenesis limit of CFFD in the NUV band (200-280 nm), we need to convert the flare energy to the NUV band via the SED model. Here, we demonstrate how to derive the CFFD needed for abiogenesis at a given planetary surface temperature. We adopt the U-band (320-400 nm), for instance, because there are previous observations for flares on

Table S3. CFFD parameters of Kepler flaring stars

KIC ID	Planet Name	α_C	β'_C
4742188	KOI-7703.01 ^a	-	-
11294822	KOI-8047.01	-1.08±0.34	35.18±11.28
5938970	Kepler-1540 b	-1.10±0.03	35.49±1.12
6497146	Kepler-438 b	-1.70±0.25	54.42±8.16
12302530	Kepler-155 c	-0.42±0.14	12.51±4.65
4762283	KOI-7706.01	-1.58±0.07	53.00±2.58
11198419	KOI-5879.01 ^b	-2.35±0.07	77.94±2.44
8424002	Kepler-1512 b	-1.64±0.01	52.12±0.41
10452252	KOI-8012.01	-1.36±0.04	44.47±1.34

^a For KIC 4742188 (KOI-7703), only one flare event was detected, so the CFFD parameters could not be fitted.

^b To calculate the total flare energy, we established an integration range from 10^{28} to 10^{38} erg for all stars, except KOI-5879. For KOI-5879, due to its minimum α_C value of -2.35, the luminosity from flares (L_{flare}) approximates the star's own luminosity (L_*) when setting the lower limit at $10^{29.85}$ erg. We therefore chose 10^{30} erg for this star as a more appropriate lower limit for flare energy, resulting in a ratio of L_{flare}/L_* equal to 0.62.

(This table is available in its entirety in machine-readable form.)

M stars, e.g., AD Leo.^{S18} The observed flare energy flux in U-band F_U can be converted to the energy flux in NUV band, i.e., the correction factor is

$$r_U = \frac{F_U}{\int_{200 \text{ nm}}^{280 \text{ nm}} F_{\text{flare}}(\lambda) d\lambda}. \quad (\text{S14})$$

For G type star like KOI-7703, $r_U = 1.94$, while for M type star like KOI-8012, $r_U = 1.19$. Considering the NUV flux due to flares dominates for M stars, we can ignore the flux for the quiet star. For a surface temperature of T_{surf} , the required energy for abiogenesis in NUV band is $F_0 \times e^{(T_{\text{surf}} - 273 \text{ K})/10 \text{ K}}$, where $F_0 = 8 \times 10^{27} \text{ erg s}^{-1}$ is the required flux according to Equation 3. Thus, for a given T_{surf} of a planet located a_p from the star, we can obtain a CFFD limit in U-band for flaring stars as follows,

$$v \geq \frac{8 \times 10^{27} \text{ erg s}^{-1}}{E_U} \left(\frac{a_p}{1 \text{ AU}}\right)^2 \times e^{(T_{\text{surf}} - 273 \text{ K})/10 \text{ K}} \times \frac{r_U}{\eta}, \quad (\text{S15})$$

where η is the planetary atmosphere transmittance. Note for G and K stars, when the quiescent NUV flux is not ignorable, it should be deducted from F_0 . Especially, if the quiescent NUV flux is larger than F_0 , the limit is satisfied, and there is no limit for the flare frequency. Setting the surface temperature $T_{\text{surf}} = 0^\circ\text{C}$ (273 K) and $\eta = 1$, we can obtain a minimum CFFD limit,

$$v \geq 6.9 \text{ day}^{-1} \times \left(\frac{10^{32} \text{ erg}}{E_U}\right) \left(\frac{a_p}{1 \text{ AU}}\right)^2 \times r_U. \quad (\text{S16})$$

Note, if the observed CFFD in the U-band intersects with the CFFD limit, there should be enough NUV energy to drive the prebiotic chemistry for abiogenesis.

We plot the limit of CFFD in Figure 6 and Figure S8, to demonstrate the minimum requirements if the planets have a surface temperature of 0°C . Also, we plot the CFFD to achieve the flux twice that of the Archean Earth, i.e., $2 \times 5,200 \text{ erg cm}^{-2} \text{ s}^{-1}$ for reference^{S24}.

Table S4. Stellar and planetary parameters of the nine Kepler stars.

The planets/candidates	T_{eff} (K)	R_* (R_{\odot})	$[Fe/H]$ (dex)	$\log g$ (dex)	M_* (M_{\odot})	Distance ^a (pc)	$f_{\text{NUV, obs}}/f_{\text{NUV, ph}}$ ^b	R_p (R_{\oplus})	Ref. ^c	T_{eq}^d (K)
Kepler-8012.01	3374_{-82}^{+112}	$0.218_{-0.06}^{+0.09}$	$-0.36_{-0.25}^{+0.30}$	$5.066_{-0.126}^{+0.103}$	$0.202_{-0.06}^{+0.111}$	$101.197_{-0.475}^{+0.479}$	452	$0.42_{-0.12}^{+0.17}$	[S26]	216
Kepler-1512 b	3484_{-91}^{+91}	$0.393_{-0.072}^{+0.048}$	$0.15_{-0.11}^{+0.11}$	$4.865_{-0.045}^{+0.077}$	$0.418_{-0.090}^{+0.051}$	$315.276_{-23.903}^{+23.903}$	402	$0.80_{-0.13}^{+0.13}$	[S27]	318
KOI-5879.01	3827_{-75}^{+56}	$0.462_{-0.07}^{+0.05}$	$-0.40_{-0.3}^{+0.1}$	$4.782_{-0.07}^{+0.06}$	$0.471_{-0.09}^{+0.06}$	$414.134_{-5.203}^{+5.229}$	365	$1.60_{-0.24}^{+0.17}$	[S28]	228
KOI-7706.01	4281_{-140}^{+115}	$0.480_{-0.064}^{+0.034}$	$-1.18_{-0.35}^{+0.3}$	$4.761_{-0.033}^{+0.077}$	$0.485_{-0.3}^{+0.046}$	$436.123_{-5.084}^{+5.203}$	7.36	$1.19_{-0.16}^{+0.08}$	[S26]	332
Kepler-155 c	4057_{-64}^{+251}	$0.529_{-0.135}^{+0.045}$	$-0.06_{-0.085}^{+0.090}$	$4.721_{-0.027}^{+0.147}$	$0.542_{-0.125}^{+0.053}$	$293.499_{-2.279}^{+2.279}$	61.4	$1.97_{-0.48}^{+0.19}$	[S27]	300
Kepler-438 b	3748_{-112}^{+112}	$0.520_{-0.061}^{+0.038}$	$0.16_{-0.14}^{+0.15}$	$4.740_{-0.029}^{+0.059}$	$0.544_{-0.041}^{+0.041}$	$179.882_{-3.128}^{+3.241}$	33.9	$1.12_{-0.17}^{+0.16}$	[S27]	320
Kepler-1540 b	4641_{-83}^{+74}	$0.747_{-0.04}^{+0.02}$	$0.16_{-0.05}^{+0.15}$	$4.557_{-0.014}^{+0.049}$	$0.734_{-0.028}^{+0.044}$	$244.960_{-0.896}^{+0.903}$	3.9	$3.14_{-0.17}^{+0.08}$	[S26]	291
KOI-8047.01	4829_{-129}^{+144}	$0.794_{-0.051}^{+0.046}$	$0.48_{-0.3}^{+0.05}$	$4.564_{-0.047}^{+0.032}$	$0.843_{-0.056}^{+0.036}$	$587.233_{-6.480}^{+6.626}$	9.4	$1.98_{-0.13}^{+0.11}$	[S26]	227
KOI-7703.01	6031_{-198}^{+180}	$0.992_{-0.111}^{+0.311}$	$-0.14_{-0.3}^{+0.03}$	$4.45_{-0.21}^{+0.07}$	$1.012_{-0.131}^{+0.144}$	$1906.89_{-118.76}^{+135.25}$	1.95	$1.96_{-0.22}^{+0.61}$	[S26]	277
The Archean Earth	5607	0.9113	0.00	4.44	1.00	1.00	1.41	1.0	-	258

^a The distance values of Kepler-438 and KOI-8047 are derived using parallaxes from GAIA DR3, ^{S29} while the distance values for other stars come from NASA Exoplanet Archive [<https://exoplanetarchive.ipac.caltech.edu/>].

^b This column lists the ratios of total NUV emission to photospheric NUV emission. The ratios of five hosts (KOI-8012, Kepler-1512, KOI-5879, Kepler-155, and KOI-8047) are measured using GALEX NUV data. For four hosts (KOI-7706, Kepler-438, Kepler-1540, and KOI-7703) without GALEX NUV and Swift UVOT observations, we estimated their ratios using the statistical values of Wang et al. ^{S11} (binned median curves in Figure S3). For the Sun, we used the solar spectrum of Willmet ^{S30} and the age evolution of NUV radiation of G-type stars to obtain the ratio of the Archean Sun with an age of 1.0 Gyr. ^{S31}

^c This column lists the references for planetary parameters.

^d The planet's equilibrium temperature (T_{eq}) is calculated assuming zero albedo and complete redistribution of heat between the day and night sides. ^{S32} (This table is available in its entirety in machine-readable form.)

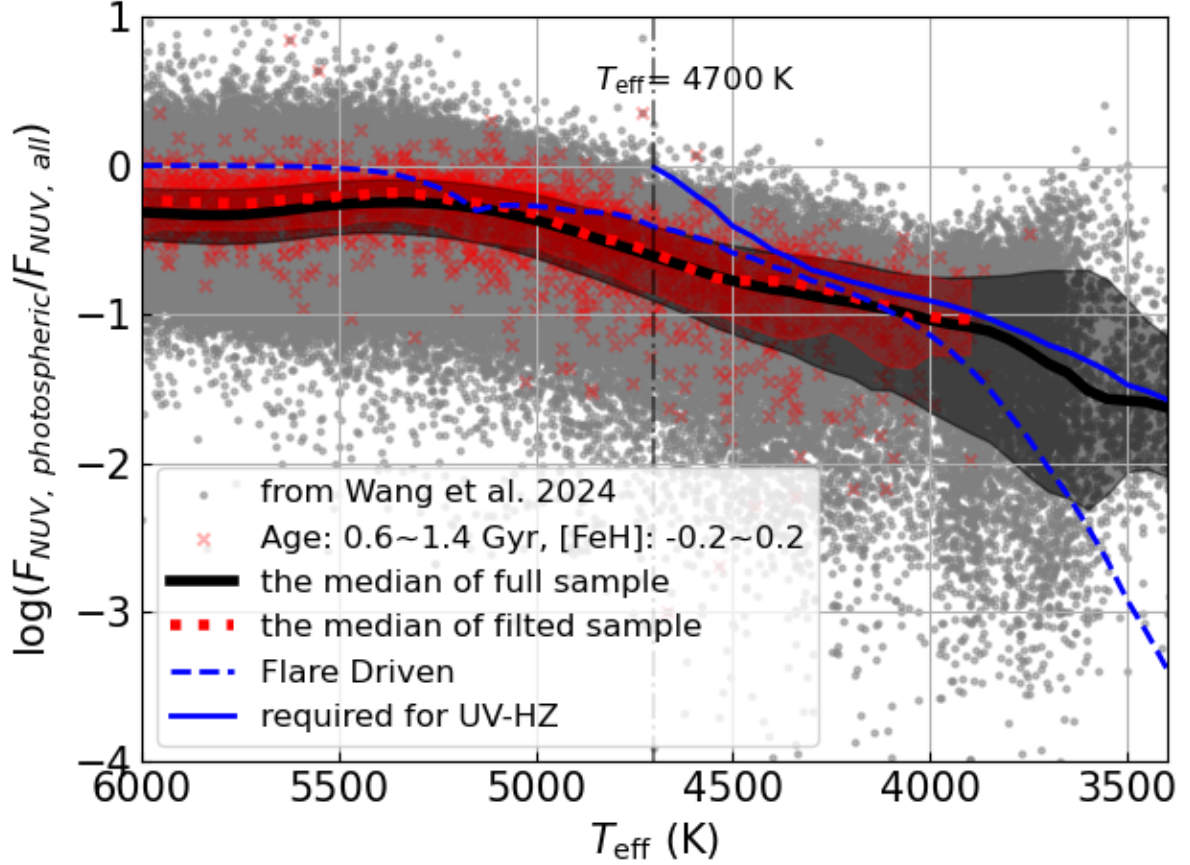


Figure S3. Ratio of photospheric emission to total emission in GALEX NUV band ($0.177\text{--}0.283\ \mu\text{m}$). The gray dots are from Wang et al.^{S11} The black line indicates the binned medians. The grey area represents the $1\text{-}\sigma$ dispersion. To examine stellar radiation with an age of 1.0 Gyr, we filtered the stars with ages from 0.6 to 1.4 Gyr and $[\text{FeH}]$ from -0.2 to $+0.2$. The selected stars are shown by pink crosses. The red dotted line indicates the binned medians of filtered samples, which are consistent with the median of the full sample. The dashed blue line indicates the ratio of the NUV radiation flux of the stellar photosphere (from the PHOENIX model) to the radiation flux driven by the flare (from this work). The blue solid line indicates the ratio of photospheric NUV radiation to total NUV radiation when the outer boundary of LW-HZ just meets the NUV radiation required by the biological mechanism (i.e., abiogenesis flux). Stars above the blue solid lines can not sustain a UV-HZ. Stars hotter than 4,700 K (separated by the black vertical dot-dashed line) have UV-HZ in the quiescent state.

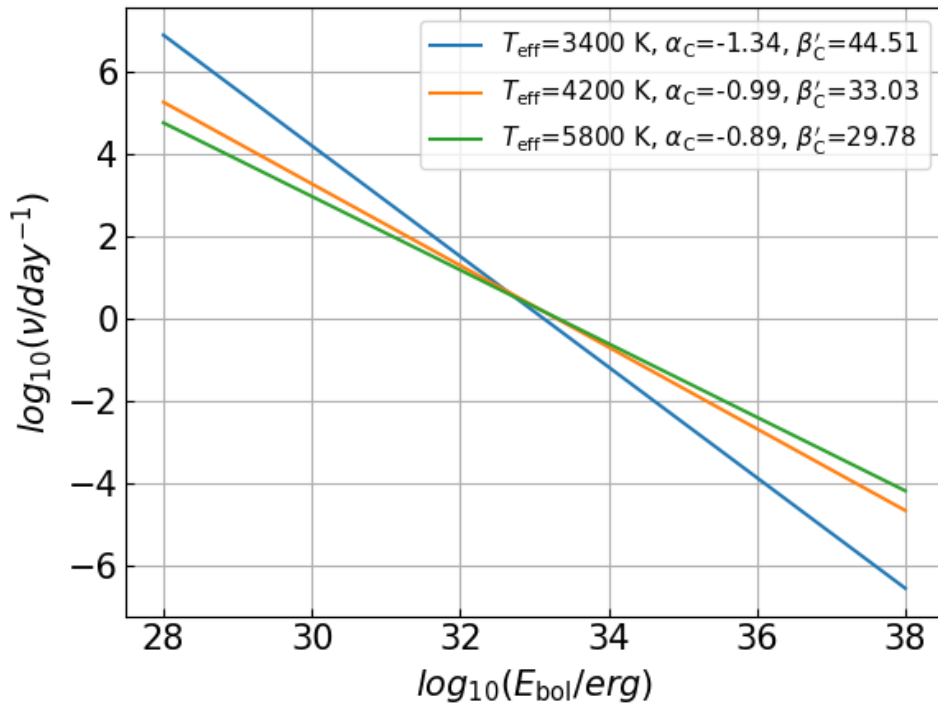


Figure S4. The CFFDs of three types of stars with temperatures of 3,400 K, 4,200 K, and 5,800 K, respectively. The power-law index α_C and β'_C are obtained from Equation S7 - S10.

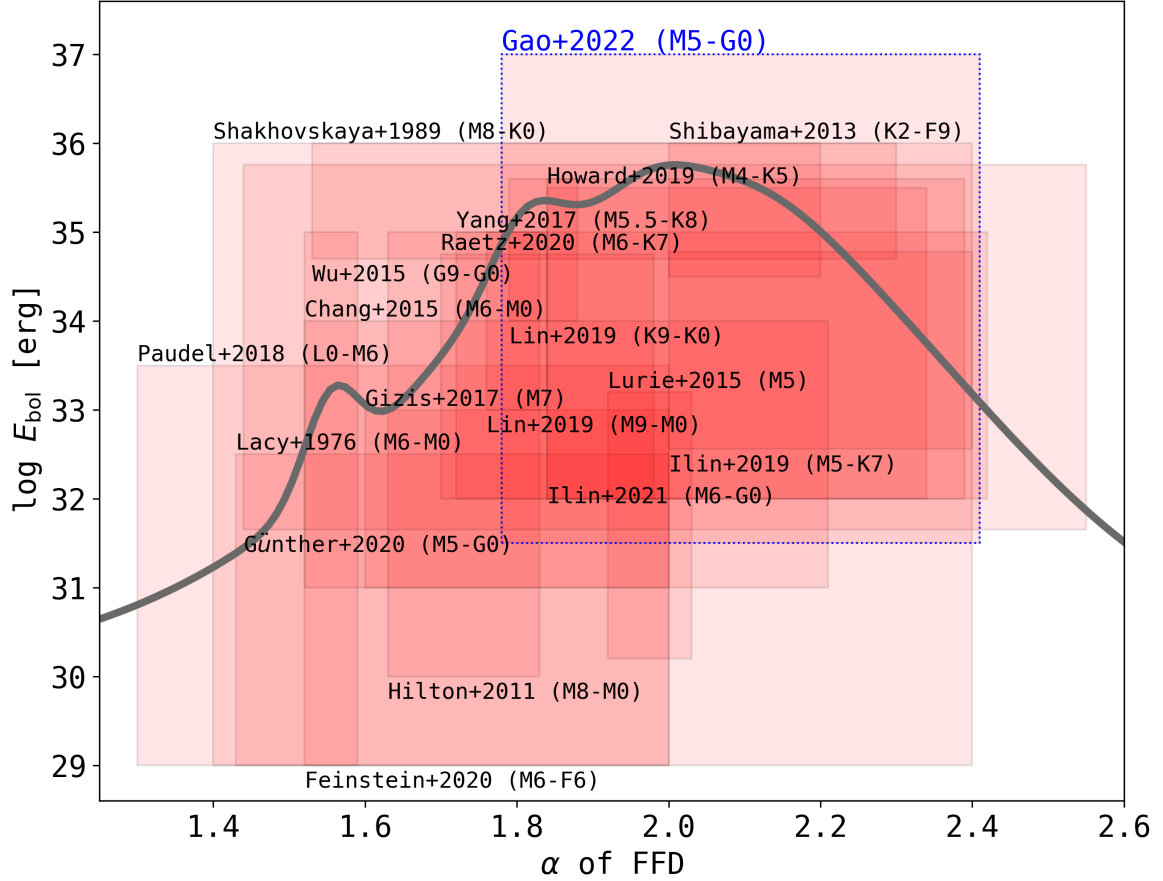


Figure S5. Overview of FFD fitting. Red rectangles indicate the flare energy range on the vertical axis and the α range on the horizontal axis, with references positioned in the upper or lower left corner of each rectangle. The gray line illustrates the superposition of these results, with each result depicted by a Gaussian fit.^{S25} The rectangle marked with a blue dashed line shows the FFD parameters used in this work, sourced from Gao et al.^{S17} Note that the value illustrated here is the positive power-law index α of the FFD, distinct from the negative power-law index of the CFFD (α_c). In the case of complete flare detection, $\alpha_c \sim -\alpha + 1$.

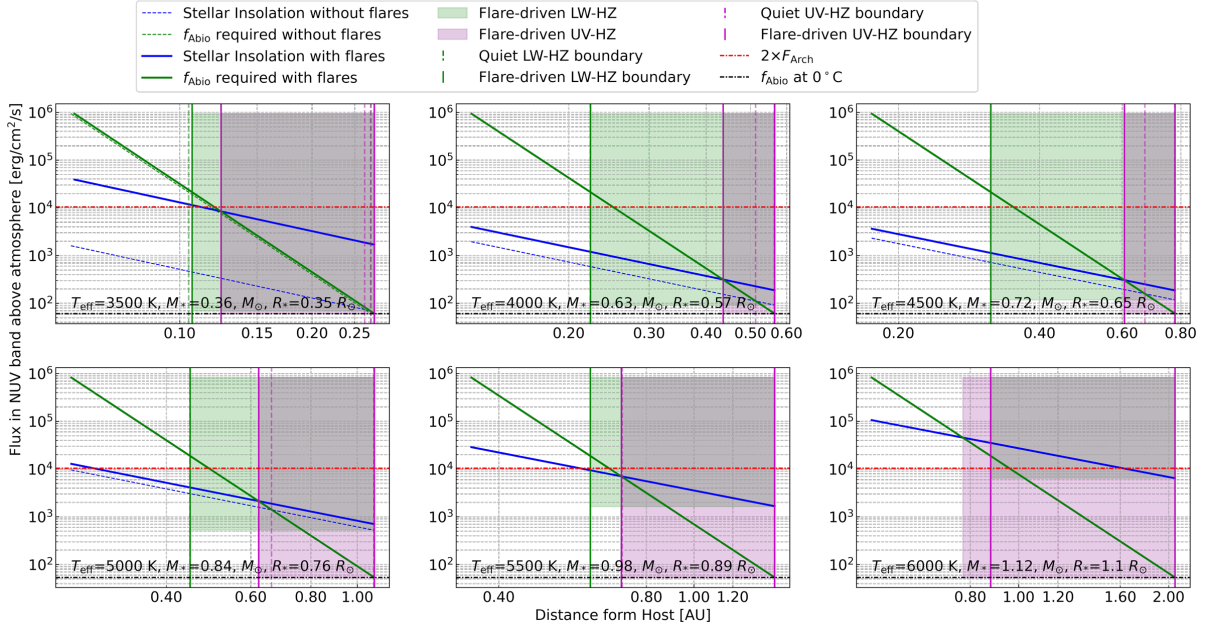


Figure S6. The flare-driven LW-HZ (green area) and UV-HZ (purple area) for flaring stars across various T_{eff} . Different colors and line styles are explained at the top. The dashed and solid blue lines represent the stellar insolation without flares and with flares, respectively. The dashed and solid green lines represent the required abiogenesis flux without flares and with flares, respectively. The dashed and solid green vertical lines represent the boundary of the LW-HZ without flares and with flares, respectively. The dashed and solid magenta vertical lines represent the boundary of the UV-HZ without flares and with flares, respectively. The dot-dashed red horizontal line represents twice the NUV flux received by the Archean Earth ($2 \times F_{\text{Arch}}$).^{S24} The dot-dashed black horizontal line represents the minimum NUV flux necessary for abiogenesis (f_{Abio}) at 0°C .^{S10} Note that the dot-dashed red and black horizontal lines are only drawn in the figure for comparison with previous work. Our definition of UV-HZ does not use the values corresponding to these two lines.

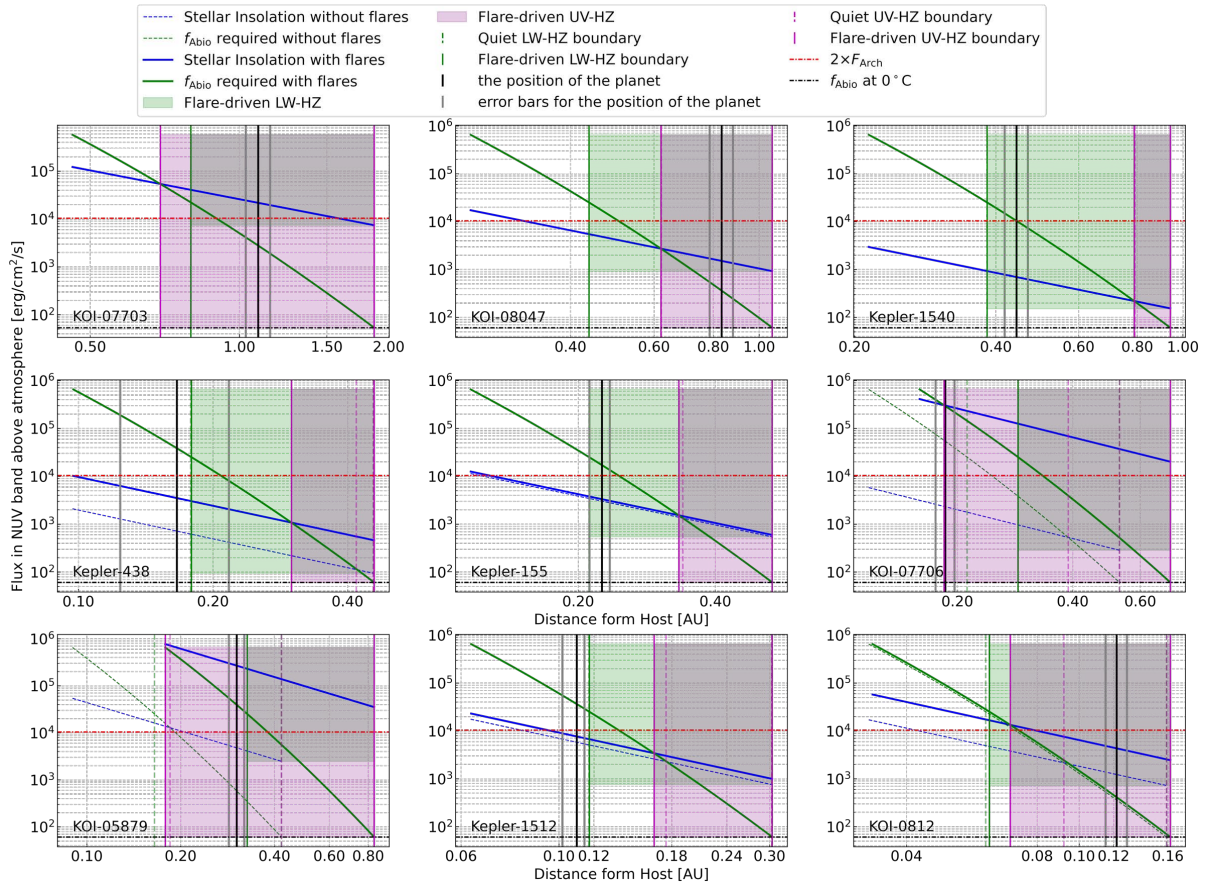


Figure S7. The flare-driven LW-HZ (green area) and UV-HZ (purple area) for flaring Kepler planetary systems analyzed in this paper. The black solid vertical lines represent the positions of planets/candidates and their error bars (gray solid vertical lines). Other colors and line styles are the same as Figure S6.

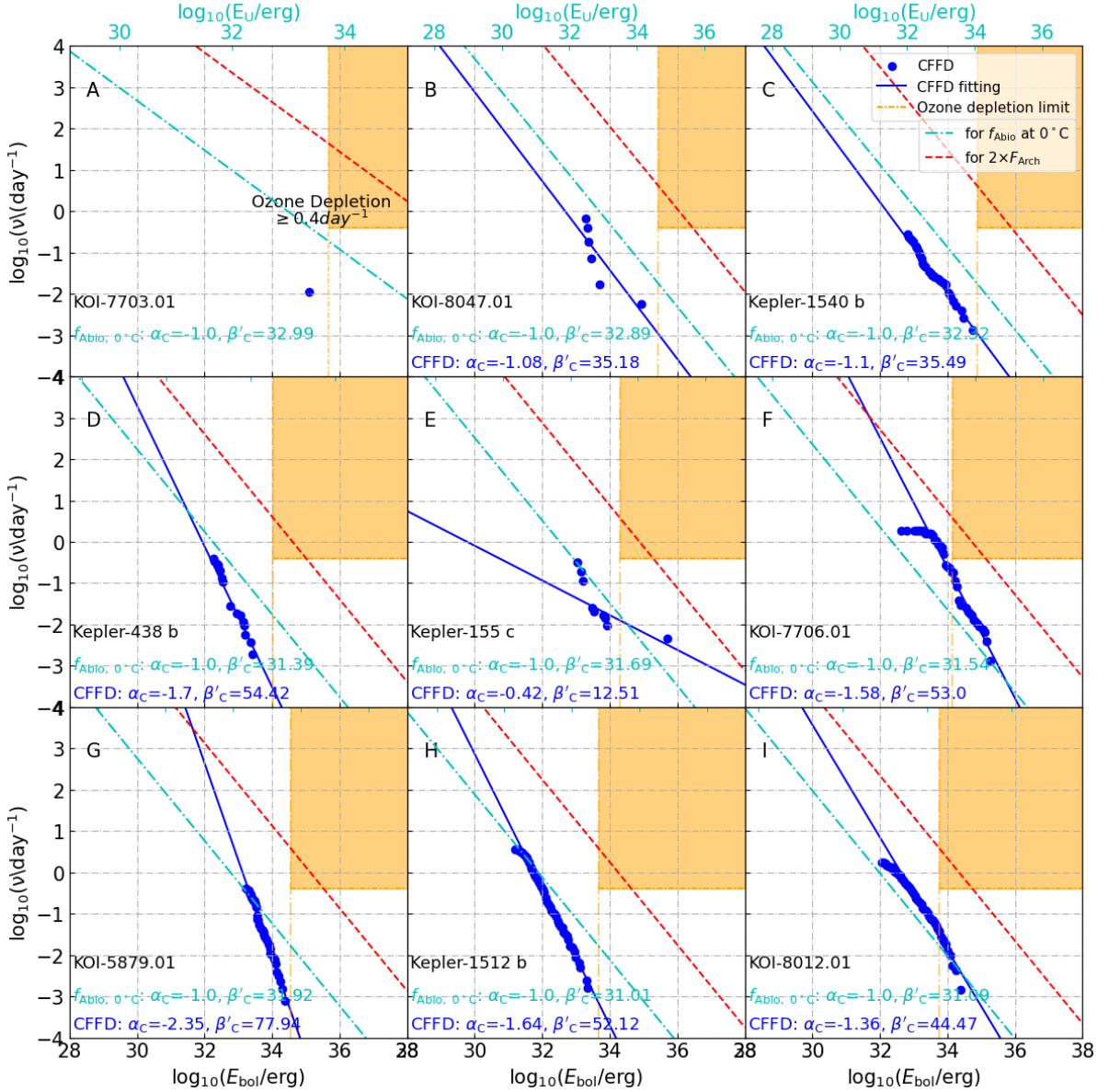


Figure S8. CFFDs of exoplanet host stars. The blue dots represent the CFFD directly from observations. The blue line illustrates the fitted CFFD, with fitted parameters (α_C and β'_C , in blue text) marked in the lower left corner of the figure. The orange area denotes the ozone depletion region, where flare frequency $\geq 0.4 \text{ day}^{-1}$ for flare bolometric energy larger than $10^{34} \times \left(\frac{d}{0.16 \text{ AU}}\right)^2 \text{ erg}$. The cyan dot-dashed line represents the minimum limit of CFFD required by the abiogenesis flux according to Equation S16. The red dashed line represents the frequency for twice the NUV flux received by the Archean Earth. For KOI-7703, only one flare was detected during Quarter 7 (89.4 days), with an energy of $1.28 \times 10^{35} \text{ erg}$, resulting in a flare frequency of approximately 0.01 day^{-1} . Note that the cyan dot-dashed and red dashed lines are only drawn in the figure for comparison with previous work. Our definition of UV-HZ does not use the values corresponding to these two lines. Since the surface temperature of a planet can vary with different atmospheric effects, the cyan line provides a minimum requirement for abiogenesis at 0°C . If the observed CFFD in the U-band intersects with the cyan line, like Kepler-438 b and Kepler-155 c, there should be enough NUV energy to drive the prebiotic chemistry on the planet. Note, the double x-axis show the bolometric flare energy E_{bol} and the flare energy in U-band E_U via the SED model in Equation 1.

Uncertainty of the calculations

Impact of Flare SEDs

We test two different flare SEDs, i.e, G0-type ($T_{\text{eff}}=6,000$ K) and M2-type ($T_{\text{eff}}=3,400$ K). No matter what the stellar type is, the variation in flare SED parameters alters the UV-HZ, as depicted in Figure S9. No matter which SEDs are adopted, the UV-HZ extended obviously, while the M2 SED leads to a closer inner boundary for all types of stars, because of the more obvious Balmer Jump in the SED model. Further spectrum observations of the flare SED are favored to determine the UV-HZ.

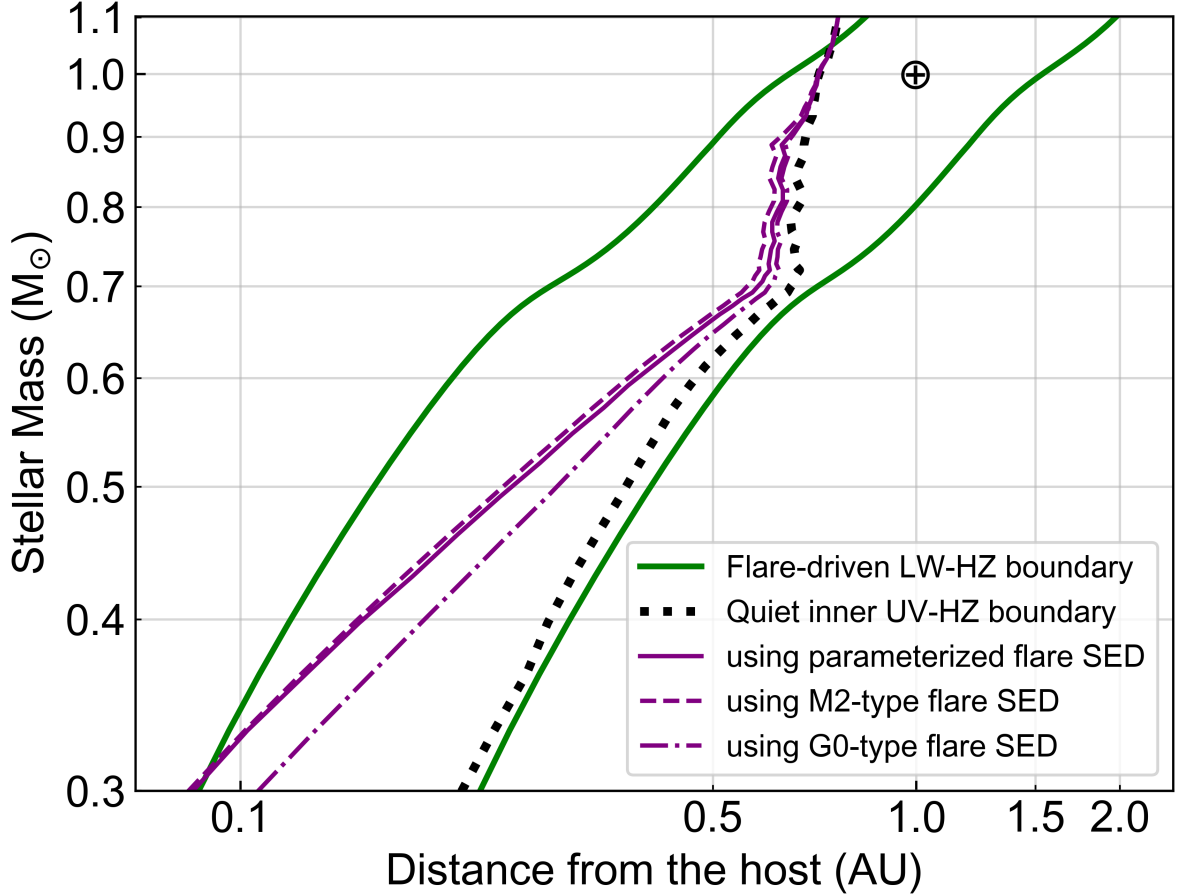


Figure S9. Change of UV-HZ and LW-HZ with different flare SEDs. The green solid lines show the inner and outer boundary of the LW-HZ with flares. The dark dotted line indicates the quiet inner boundary of UV-HZ. The purple solid line indicates the flare-driven inner boundary as determined by the parameterized flare SED model (refer to Equation 1 in the main paper). The purple dashed and dot-dashed lines illustrate the inner boundary using the M2 ($T_{\text{eff}}=3,400$ K) and G2 ($T_{\text{eff}}=6,000$ K) flare SED model, respectively. The changes in the SED influence the UV-HZ more obviously for low-mass stars. The chosen G2 SED with no Balmer jump leads to fewer NUV contributions and then has a further inner UV-HZ.

Impact of CFFDs

The CFFD of a star usually has large uncertainties. We test the influence of CFFD on the UV-HZ, using KOI-8012 as an example. The uncertainties of the two CFFD parameters are shown as the blue cross in Figure S10. In most cases, the UV-HZ can exist, with a width of ~ 0.05 AU, while for large α_C and β_C , the UV-HZ vanishes because of the limit of ozone depletion. Thus, the uncertainties of CFFD can

affect the width of UV-HZ, but the influence of the uncertainty would be limited, unless the flare energy reaches the limits of ozone depletion.

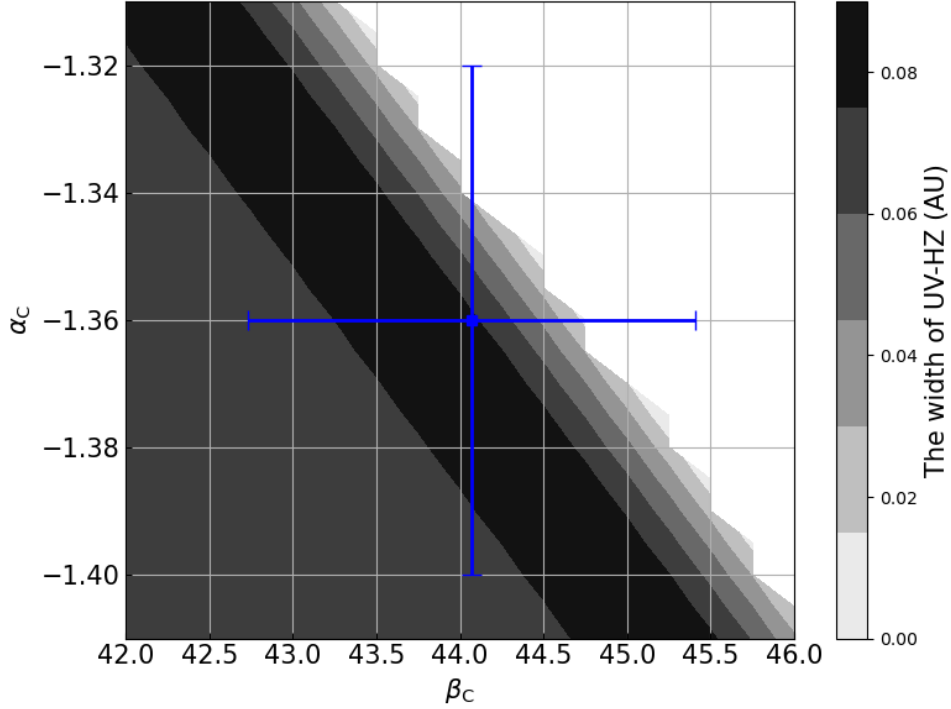


Figure S10. Variation of UV-HZ width with different CFFD parameters for KOI-8012. Blue cross indicate the α_C and β_C values for KOI-8012, obtained using the method of Gao et al.^{S17} Here, we artificially cut the ozone depletion limit. When the β_C increases by ~ 0.7 , or α_C increases by 0.2, the width of UV-HZ decreases from ~ 0.09 AU to 0 AU, and disappear. However, for most cases inside the 1-sigma uncertainty, the UV-HZ can sustain with a width larger than 0.05 AU.

The values and uncertainties of the CFFD parameters α_C and β'_C are listed in Table S3 for nine *Kepler* flaring hosts. To determine the UV-HZ width in an accurate way, both flare SEDs and the CFFDs need to be measured or modeled more precisely.

Additionally, when we estimate the increases of NUV flux due to flares via Equation S5, the upper and lower energy limits we choose will affect the total integrated energy due to flares. Since most of $\alpha_C < -1$, the flares with low energy will dominantly contribute to the total energy. Thus, we test different choices for the lower energy limit. Figure S11 shows how the UV-HZ varies when a low-energy flare changes from 10^{28} to 10^{32} erg. The results of G stars are not sensitive to the choices, while for M stars, the choices become important. Even with a higher limit as high as 10^{32} erg, the UV-HZ expanded by an average of ~ 0.05 AU. As the detection of low-energy flares becomes more complete, the UV-HZ expands to the inner region.

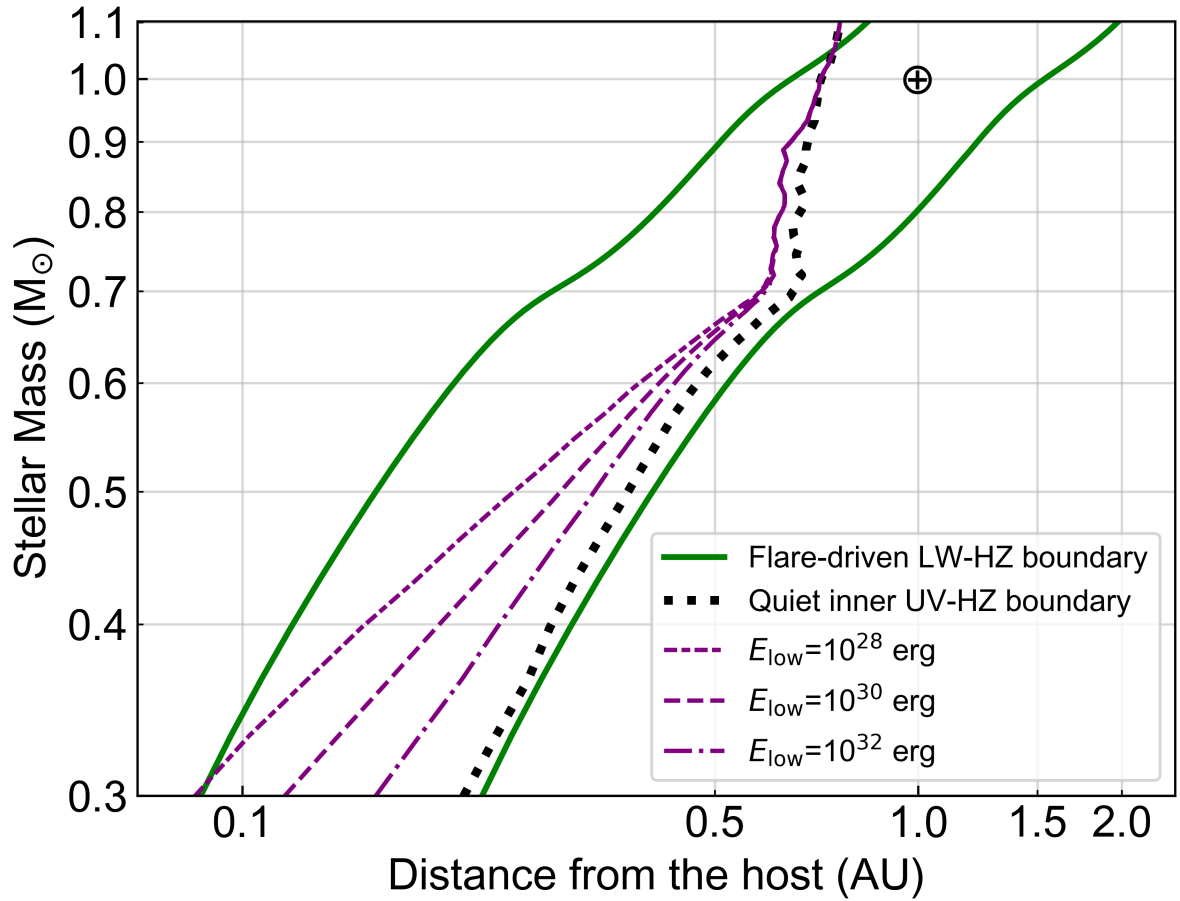


Figure S11. Variation of the UV-HZ with the lower energy threshold of flare detection. The flare-driven inner boundary of UV-HZ is shown for flare energies down to 10^{28} erg (short-dashed), 10^{30} erg (long-dashed), and 10^{32} erg (dot-dashed). Other colors and line styles are the same as Figure S9.

Supplemental References

- S1. Kowalski, A. F., Allred, J. C., Uitenbroek, H., et al. (2017). Hydrogen Balmer Line Broadening in Solar and Stellar Flares. *The Astrophysical Journal* **837**: 125. DOI: [10.3847/1538-4357/aa603e](https://doi.org/10.3847/1538-4357/aa603e).
- S2. Brasseur, C. E., Osten, R. A., Tristan, I. I., et al. (2023). Constraints on Stellar Flare Energy Ratios in the NUV and Optical from a Multiwavelength Study of GALEX and Kepler Flare Stars. *The Astrophysical Journal* **944**: 5. DOI: [10.3847/1538-4357/acab59](https://doi.org/10.3847/1538-4357/acab59).
- S3. Jackman, J. A. G., Shkolnik, E. L., Million, C., et al. (2023). Extending optical flare models to the UV: results from comparing of TESS and GALEX flare observations for M Dwarfs. *Monthly Notices of the Royal Astronomical Society* **519**: 3564–3583. DOI: [10.1093/mnras/stac3135](https://doi.org/10.1093/mnras/stac3135).
- S4. Segura, A., Walkowicz, L. M., Meadows, V., et al. (2010). The Effect of a Strong Stellar Flare on the Atmospheric Chemistry of an Earth-like Planet Orbiting an M Dwarf. *Astrobiology* **10**: 751–771. DOI: [10.1089/ast.2009.0376](https://doi.org/10.1089/ast.2009.0376).
- S5. Kowalski, A. F. (2022). Near-Ultraviolet Continuum Modeling of the 1985 April 12 Great Flare of AD Leo. *Frontiers in Astronomy and Space Sciences* **9**: 351. DOI: [10.3389/fspas.2022.1034458](https://doi.org/10.3389/fspas.2022.1034458).
- S6. Fleming, S. W., Million, C., Osten, R. A., et al. (2022). New Time-resolved, Multi-band Flares in the GJ 65 System with gPhoton. *The Astrophysical Journal* **928**: 8. DOI: [10.3847/1538-4357/ac5037](https://doi.org/10.3847/1538-4357/ac5037).
- S7. Berger, V. L., Hinkle, J. T., Tucker, M. A., et al. (2024). Stellar flares are far-ultraviolet luminous. *Monthly Notices of the Royal Astronomical Society* **532**: 4436–4445. DOI: [10.1093/mnras/stae1648](https://doi.org/10.1093/mnras/stae1648).
- S8. Kowalski, A. F., Wisniewski, J. P., Hawley, S. L., et al. (2019). The Near-ultraviolet Continuum Radiation in the Impulsive Phase of HF/GF-type dMe Flares. I. Data. *The Astrophysical Journal* **871**: 167. DOI: [10.3847/1538-4357/aaf058](https://doi.org/10.3847/1538-4357/aaf058).
- S9. Howard, W. S., Corbett, H., Law, N. M., et al. (2020). EvryFlare. III. Temperature Evolution and Habitability Impacts of Dozens of Superflares Observed Simultaneously by Evryscope and TESS. *The Astrophysical Journal* **902**: 115. DOI: [10.3847/1538-4357/abb5b4](https://doi.org/10.3847/1538-4357/abb5b4).
- S10. Rimmer, P. B., Xu, J., Thompson, S. J., et al. (2018). The origin of RNA precursors on exoplanets. *Science Advances* **4**: eaar3302. DOI: [10.1126/sciadv.aar3302](https://doi.org/10.1126/sciadv.aar3302).
- S11. Wang, S., Li, X., Han, H., et al. (2024). Predicting Photospheric Ultraviolet Emission from Stellar Evolutionary Models. *The Astrophysical Journal* **976**: 43. DOI: [10.3847/1538-4357/ad87d0](https://doi.org/10.3847/1538-4357/ad87d0).
- S12. Wang, J.-H., Xiang, M., Zhang, M., et al. (2025). Spectroscopic Ages for 4 Million Main-sequence Dwarf Stars from LAMOST DR10 Estimated with a Data-driven Approach. *The Astrophysical Journal Supplement Series* **280**: 13. DOI: [10.3847/1538-4365/aded16](https://doi.org/10.3847/1538-4365/aded16).

- S13. Shibata, K. and Magara, T. (2011). Solar Flares: Magnetohydrodynamic Processes. *Living Reviews in Solar Physics* **8**: 6. DOI: [10.12942/lrsp-2011-6](https://doi.org/10.12942/lrsp-2011-6).
- S14. Yang, H. and Liu, J. (2019). The Flare Catalog and the Flare Activity in the Kepler Mission. *The Astrophysical Journal Supplement Series* **241**: 29. DOI: [10.3847/1538-4365/ab0d28](https://doi.org/10.3847/1538-4365/ab0d28).
- S15. Günther, M. N., Zhan, Z., Seager, S., et al. (2020). Stellar Flares from the First TESS Data Release: Exploring a New Sample of M Dwarfs. *The Astronomical Journal* **159**: 60. DOI: [10.3847/1538-3881/ab5d3a](https://doi.org/10.3847/1538-3881/ab5d3a).
- S16. Tu, Z.-L., Yang, M., Zhang, Z. J., et al. (2020). Superflares on Solar-type Stars from the First Year Observation of TESS. *The Astrophysical Journal* **890**: 46. DOI: [10.3847/1538-4357/ab6606](https://doi.org/10.3847/1538-4357/ab6606).
- S17. Gao, D.-Y., Liu, H.-G., Yang, M., et al. (2022). Correcting Stellar Flare Frequency Distributions Detected by TESS and Kepler. *The Astronomical Journal* **164**: 213. DOI: [10.3847/1538-3881/ac937e](https://doi.org/10.3847/1538-3881/ac937e).
- S18. Hawley, S. L., Davenport, J. R. A., Kowalski, A. F., et al. (2014). Kepler Flares. I. Active and Inactive M Dwarfs. *The Astrophysical Journal* **797**: 121. DOI: [10.1088/0004-637X/797/2/121](https://doi.org/10.1088/0004-637X/797/2/121).
- S19. Paudel, R. R., Gizis, J. E., Mullan, D. J., et al. (2018). K2 Ultracool Dwarfs Survey. III. White Light Flares Are Ubiquitous in M6-L0 Dwarfs. *The Astrophysical Journal* **858**: 55. DOI: [10.3847/1538-4357/aab8fe](https://doi.org/10.3847/1538-4357/aab8fe).
- S20. Jackman, J. A. G., Wheatley, P. J., Acton, J. S., et al. (2021). Stellar flares detected with the Next Generation Transit Survey. *Monthly Notices of the Royal Astronomical Society* **504**: 3246–3264. DOI: [10.1093/mnras/stab979](https://doi.org/10.1093/mnras/stab979).
- S21. Mamajek, E. E. and Hillenbrand, L. A. (2008). Improved Age Estimation for Solar-Type Dwarfs Using Activity-Rotation Diagnostics. *The Astrophysical Journal* **687**: 1264–1293. DOI: [10.1086/591785](https://doi.org/10.1086/591785).
- S22. Fouesneau, M., Frémat, Y., Andrae, R., et al. (2023). Gaia Data Release 3. Apsis. II. Stellar parameters. *Astronomy & Astrophysics* **674**: A28. DOI: [10.1051/0004-6361/202243919](https://doi.org/10.1051/0004-6361/202243919).
- S23. Baraffe, I., Homeier, D., Allard, F., et al. (2015). New evolutionary models for pre-main sequence and main sequence low-mass stars down to the hydrogen-burning limit. *Astronomy & Astrophysics* **577**: A42. DOI: [10.1051/0004-6361/201425481](https://doi.org/10.1051/0004-6361/201425481).
- S24. Buccino, A. P., Lemarchand, G. A., and Mauas, P. J. D. (2006). Ultraviolet radiation constraints around the circumstellar habitable zones. *Icarus* **183**: 491–503. DOI: [10.1016/j.icarus.2006.03.007](https://doi.org/10.1016/j.icarus.2006.03.007).
- S25. Ilin, E., Schmidt, S. J., Poppenhäger, K., et al. (2021). Flares in open clusters with K2. II. Pleiades, Hyades, Praesepe, Ruprecht 147, and M 67. *Astronomy & Astrophysics* **645**: A42. DOI: [10.1051/0004-6361/202039198](https://doi.org/10.1051/0004-6361/202039198).

- S26. Thompson, S. E., Coughlin, J. L., Hoffman, K., et al. (2018). Planetary Candidates Observed by Kepler. VIII. A Fully Automated Catalog with Measured Completeness and Reliability Based on Data Release 25. *The Astrophysical Journal Supplement Series* **235**: 38. DOI: [10.3847/1538-4365/aab4f9](https://doi.org/10.3847/1538-4365/aab4f9).
- S27. Torres, G., Kane, S. R., Rowe, J. F., et al. (2017). Validation of Small Kepler Transiting Planet Candidates in or near the Habitable Zone. *The Astronomical Journal* **154**: 264. DOI: [10.3847/1538-3881/aa984b](https://doi.org/10.3847/1538-3881/aa984b).
- S28. Mullally, F., Coughlin, J. L., Thompson, S. E., et al. (2015). Planetary Candidates Observed by Kepler. VI. Planet Sample from Q1–Q16 (47 Months). *The Astrophysical Journal Supplement Series* **217**: 31. DOI: [10.1088/0067-0049/217/2/31](https://doi.org/10.1088/0067-0049/217/2/31).
- S29. Gaia Collaboration (2022). VizieR Online Data Catalog: Gaia DR3 Part 1. Main source (Gaia Collaboration, 2022). VizieR Online Data Catalog, I/355. DOI: [10.26093/cds/vizier.1355](https://doi.org/10.26093/cds/vizier.1355).
- S30. Willmer, C. N. A. (2018). The Absolute Magnitude of the Sun in Several Filters. *The Astrophysical Journal Supplement Series* **236**: 47. DOI: [10.3847/1538-4365/aabfdf](https://doi.org/10.3847/1538-4365/aabfdf).
- S31. Li, X., Wang, S., Ma, J., et al. (2025). Evolution of Stellar Activity and Habitable Zone. I. Ultraviolet Emission of Dwarfs in Open Clusters and Field Stars. *The Astrophysical Journal Supplement Series* **281**: 13. DOI: [10.3847/1538-4365/ae08a9](https://doi.org/10.3847/1538-4365/ae08a9).
- S32. Kempton, E. M. .-, Bean, J. L., Louie, D. R., et al. (2018). A Framework for Prioritizing the TESS Planetary Candidates Most Amenable to Atmospheric Characterization. *Publications of the Astronomical Society of the Pacific* **130**: 114401. DOI: [10.1088/1538-3873/aadf6f](https://doi.org/10.1088/1538-3873/aadf6f).